


# The giant 1960 tsunami in the context of a 6000-year record of paleotsunamis and coastal evolution in south-central Chile

Pedro I. Matos-Llavona<sup>1,2</sup>  | Lisa L. Ely<sup>2</sup> | Breanyn MacInnes<sup>2</sup> | Tina Dura<sup>3</sup> | Marco A. Cisternas<sup>4</sup> | Joanne Bourgeois<sup>5</sup> | David Bruce<sup>3,2</sup> | Jessica DePaolis<sup>3</sup> | Alexander Dolcimascolo<sup>6,2</sup> | Benjamin P. Horton<sup>7</sup> | Daniel Melnick<sup>8</sup> | Alan R. Nelson<sup>9</sup> | Walter Szeliga<sup>2</sup> | Robert L. Wesson<sup>9</sup>

<sup>1</sup>Department of Geosciences, University of Massachusetts Amherst, Amherst, MA, USA

<sup>2</sup>Department of Geological Sciences, Central Washington University, Ellensburg, WA, USA

<sup>3</sup>Department of Geosciences, Virginia Polytechnic Institute and State University, Blacksburg, VA, USA

<sup>4</sup>Instituto de Geografía, Pontificia Universidad Católica de Valparaíso, Valparaíso, Chile

<sup>5</sup>Department of Earth & Space Sciences, University of Washington, Seattle, WA, USA

<sup>6</sup>Washington Geological Survey, Washington State Department of Natural Resources, Olympia, WA, USA

<sup>7</sup>Earth Observatory of Singapore, Nanyang Technological University, Singapore

<sup>8</sup>Instituto de Ciencias de la Tierra, Universidad Austral de Chile, Valdivia, Chile

<sup>9</sup>Geologic Hazards Science Center, U.S. Geological Survey, Golden, CO, USA

## Correspondence

Pedro I. Matos-Llavona, Department of Geosciences, University of Massachusetts Amherst, 249 Morrill Science Center, 611 North Pleasant Street, Amherst, MA 01003, USA.

Email: pmatosllavon@umass.edu

## Funding information

Puget Sound Energy Graduate Fellowship at Central Washington University; Earthquake Hazards Program of the U.S. Geological Survey; Chilean National Fund for Development of Science and Technology (FONDECYT), Grant/Award Numbers: 1190258, 1181479; Millennium Scientific Initiative (ICM) of the Chilean government, Grant/Award Number: NC160025; National Science Foundation (NSF), Grant/Award Numbers: EAR-1624533, EAR-1624542; ANID PIA Anillo, Grant/Award Number: ACT192169

## Abstract

The tsunami associated with the giant 9.5  $M_w$  1960 Chile earthquake deposited an extensive sand layer above organic-rich soils near Queule (39.3°S, 73.2°W), south-central Chile. Using the 1960 tsunami deposits, together with eye-witness observations and numerical simulations of tsunami inundation, we tested the tsunami inundation sensitivity of the site to different earthquake slip distributions. Stratigraphically below the 1960 deposit are two additional widespread sand layers interpreted as tsunami deposits with maximum ages of 4960–4520 and 5930–5740 cal BP. This >4500-year gap of tsunami deposits preserved in the stratigraphic record is inconsistent with written and geological records of large tsunamis in south-central Chile in 1575, 1837, and possibly 1737. We explain this discrepancy by: (1) poor preservation of tsunami deposits due to reduced accommodation space from relative sea-level fall during the late Holocene; (2) recently evolved coastal geomorphology that increased sediment availability for tsunami deposit formation in 1960; and/or (3) the possibility that the 1960 tsunami was significantly larger at this particular location than other tsunamis in the past >4500 years. Our research illustrates the complexities of reconstructing a complete stratigraphic record of past tsunamis from a single site for tsunami hazard assessment.

## KEYWORDS

Chile 1960 earthquake, coastal geomorphology, coastal hazard, earthquake geomorphology, paleoseismology, tsunami deposits

## 1 | INTRODUCTION

Large megathrust earthquakes and tsunamis constitute major hazards for coastal communities near subduction zones. Yet, the low frequency of these events and sparse historical records of them limit our ability to identify their spatial and temporal patterns. These limitations can be partially overcome using sedimentary evidence of megathrust tsunamis preserved in coastal stratigraphy (e.g. Atwater et al., 1995; Cisternas et al., 2005; Clark et al., 2019; Ely et al., 2014; MacInnes et al., 2010; Rubin et al., 2017; Satake & Atwater, 2007; Sawai et al., 2012; Witter et al., 2019).

Reconstructing a history of great megathrust earthquakes from the deposits of their tsunamis at sites behind a coastal barrier, such as a dune ridge, presents problems. The deposition from a tsunami depends on multiple, often interconnected factors, including: (1) tsunami height; (2) site exposure to inundation; (3) sediment availability; (4) preservation potential of deposits; (5) changes in relative sea level (RSL) in the Holocene; and (6) geomorphic evolution of the coast (Dura et al., 2016; Szczuciński, 2012). Although these factors pose challenges for reconstructing events at individual sites, multiple sites with independent earthquake histories can help constrain the locations and timing of source earthquakes and increase understanding of the role of the geomorphic evolution of the coast (Garrett et al., 2020; Nelson et al., 2021; Philiposian & Meltzner, 2020; Sawai, 2020; Shennan et al., 2014).

The historical record of earthquakes and tsunamis in south-central Chile since the arrival of the Spanish in 1541—together with relatively long tidal marsh (~2000 years at Maullín; Cisternas et al., 2005) and lacustrine (>5000 years; Kempf et al., 2017; Moernaut et al., 2014) records of past earthquakes and tsunamis—presents an opportunity to develop prehistoric earthquake and tsunami histories for the late Holocene. Here we analysed sedimentary evidence of the giant  $M_w$  9.51960 Chile earthquake and two previous instances of tsunami inundation over the last ~6000 years near Queule, south-central Chile (Figure 1). Using the 1960 tsunami deposits, together with eye-witness observations and numerical simulations of tsunami inundation, we test the tsunami inundation sensitivity of the site to different earthquake slip distributions. We then compare our longer record of tsunami inundation near Queule to other regional records of great earthquakes and tsunamis and consider the role of the geomorphic evolution and sea-level change at the site in the preservation of tsunami deposits.

## 1.1 | Background

## 1.1.1 | Geologic setting and earthquake history

South-central Chile lies along the Chilean trench and the convergent plate boundary between the Nazca oceanic and the South American

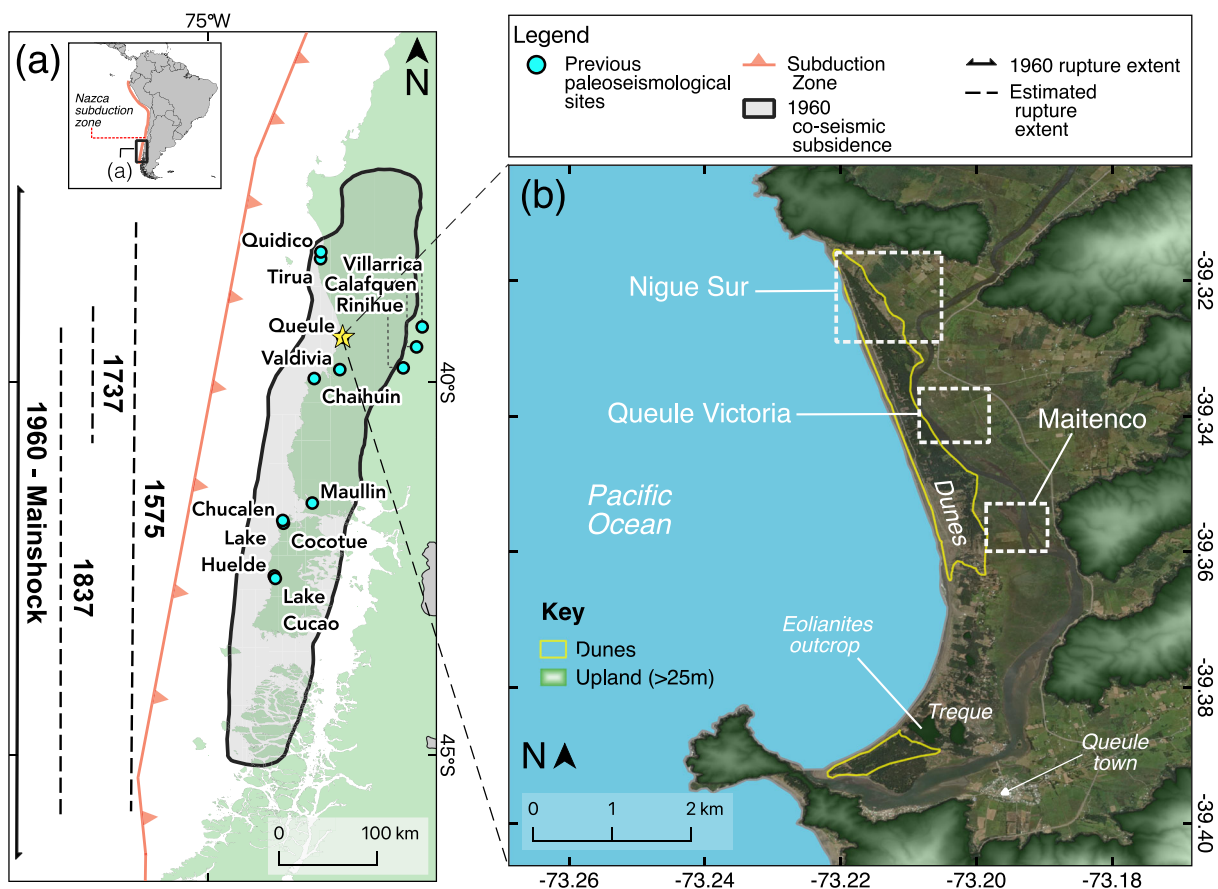


**FIGURE 1** (a) Location and tectonic setting map of south-central Chile showing locations of previous paleoseismology studies (Cisternas et al., 2005, 2017a,b; Dura et al., 2015, 2017; Ely et al., 2014; Garrett et al., 2015; Hong et al., 2017; Kempf et al., 2015, 2017, 2020; Moernaut et al., 2014, 2018). The longitudinal dashed lines represent the along-strike rupture extent of major historical earthquakes in south-central Chile. The shaded region shows the area of co-seismic land-level subsidence during the 1960 earthquake (Plafker & Savage, 1970). (b) Map of Queule site with study locations outlined by dashed lines

continental plates (Figure 1). The Nazca plate subducts beneath the South American plate at an average rate of 6.6 cm/yr (Angermann et al., 1999), resulting in multiple great ( $M_w > 8.0$ ) historical earthquakes and tsunamis, including the largest earthquake recorded with modern instrumentation: the 1960  $M_w$  9.5 earthquake (Barrientos & Ward, 1990; Bilek, 2010; Cifuentes, 1989; Ruiz & Madariaga, 2018).

Stratigraphic evidence at sites along the Chilean coast extends the record of great earthquakes as far back as  $\sim 6$  ka (Kempf et al., 2017). The significant spatial variability in the timing and frequency of these earthquakes (Bilek, 2010) may result from segmentation of the megathrust zone at the Arauco peninsula ( $38^\circ\text{S}$ ), dividing the central Chile segment from the south-central Valdivia segment at the northern boundary of the 1960 earthquake rupture (Dura et al., 2017; Melnick et al., 2009; Moreno et al., 2011).

The 1960  $M_w$  9.5 south Chile earthquake ruptured  $920 \pm 100$  km of the southern segment of the Chilean trench (Cifuentes, 1989; Figure 1). A series of  $M_w$  7.0 precursors near the Arauco peninsula on 21 May 1960 was followed by the  $M_w$  9.5 main shock on 22 May (Watanabe & Kokot, 1960; Weischet, 1960). The earthquake caused major damage to infrastructure and an estimated 490–5700 casualties in Chile, as well as widespread landslides, fissures, and liquefaction (Duke & Leeds, 1963; National Centers for Environmental Information, 2019; Reinhardt et al., 2009; Weischet, 1963; Wright & Mella, 1963). The main shock produced co-seismic subsidence of up to 2 m in an area stretching 1000 km along the coast and up to 200 km inland in the southern portion of the rupture zone (Plafker & Savage, 1970; Figure 1). The resulting tsunami caused significant coastal inundation and damaged all ports from north of Concepción to Chiloé Island (Figure 1; Sievers et al., 1963; Wright & Mella, 1963). The tsunami runup reached elevations of 15 m near Ancud in northern Chiloé Island ( $41.86^\circ\text{S}$ ,  $73.82^\circ\text{W}$ ) and 8 m in Corral, near Valdivia (Figure 1; Sievers et al., 1963). The waves crossed the Pacific and achieved runup elevations of 10 m in Hawai'i (Eaton et al., 1961) and 6 m in Japan and Kamchatka (Abe, 1979; Zayakin & Luchinina, 1987).

Three major historical earthquakes in 1575, 1737, and 1837 CE preceded the 1960 CE earthquake along the southern segment of the Chilean trench (Cisternas, Carvajal, et al., 2017; Ruiz & Madariaga, 2018; Figure 1). The 1575 earthquake and tsunami closely resembled the 1960 earthquake and tsunami—in magnitude and extent—as determined from stratigraphic and historical evidence (Cisternas, Carvajal, et al., 2017). Although the 1737 earthquake damaged towns from Valdivia to Isla Chiloé (Lomnitz, 2004), the only evidence of a tsunami is a deposit reported at Chaihuín (Aedo et al., 2021; Hocking et al., 2021). Mapping and dating of lake turbidites suggest that the fault rupture in 1737 was confined to the northern half of the 1960 rupture zone (Figure 1; Moernaut et al., 2014). The estimated magnitude of the 1837 earthquake is between 8.8 and 9.5  $M_w$ , inferred from historical accounts of shaking intensity and location, land-level changes, and tsunami waves in Chile, Hawai'i, and Japan (Abe, 1979; Cisternas, Carvajal, et al., 2017). Evidence from sandy tsunami deposits, subsided wetlands, and inland lake turbidites suggests that the rupture in 1837 was confined to the southern portion of the 1960 rupture zone (Figure 1; Cisternas

et al., 2005; Cisternas, Carvajal, et al., 2017; Kempf et al., 2015, 2017; Moernaut et al., 2014).

### 1.1.2 | Study area

Our study area consists of three sites near the coastal town of Queule ( $39.3^\circ\text{S}$ ,  $73.2^\circ\text{W}$ ) in south-central Chile. This area was chosen with the aim of refining the along-strike rupture extents of earthquakes along the southern segment of the Chilean trench (Figure 1). Queule is 50 km north of Valdivia (Figure 1) and bounded to the north, south, and east by Pre-Cambrian metamorphic bedrock headlands and to the west by a sand spit capped by eolian sand dunes and the Pacific Ocean (Figure 1; Pino & Muslow, 1983). The low-energy, estuarine Queule River flows southward inland of the sand spit and is influenced by tides with a maximum tidal range of 1.5 m. The alluvial sediment is mainly very fine sand and mud with a mineralogical composition suggesting a local metamorphic bedrock source (Pino & Muslow, 1983; Rohas, 1986).

We targeted Queule due to: (1) available accounts of the 1960 earthquake and tsunami by local residents (see Table SI-1 in the online Supporting Information); (2) prior descriptions of the 1960 and older tsunami deposits (W. Manley, A. Nelson, & J. Bourgeois, unpublished data, 1989); and (3) proximity to the city of Valdivia (55 km), which has a record of earthquakes and tsunamis since 1575. Specific sites near Queule, namely Nigue Sur, Queule Victoria, and Maitenco, were selected as having high preservation potential, protection from erosion, a potential sediment source (e.g. beach and dunes), and promising core stratigraphy based on an examination of satellite imagery and aerial photographs from 1944, 1961, 1979, and 1983, as well as unpublished 1989 stratigraphic descriptions of cores near Maitenco (Figure 1).

Nigue Sur is a pasture with patches of native vegetation forests bounded by upland bedrock to the north, eolian sand dunes to the west, and the Queule River to the east. Queule Victoria and Maitenco sites (Figure 1) are a pasture and low marsh, respectively, located on the eastern bank of the Queule River across from the location where the modern barrier sand dunes have the lowest elevation.

Near the town of Queule (Figure 1), witnesses reported that the 1960 tsunami breached the coastal dunes in multiple locations along the coast (see Tables SI-1 and SI-2). The second wave destroyed Queule (Figure 2), leaving a debris line 2 km inland and killing 35 people (Weischet, 1960). A minimum tsunami flow depth of 4–4.5 m above ground surface was estimated from floating debris caught in trees 1.5 km inland from the coast near Queule (Weischet, 1960, 1963). A sand fan blocked the Queule River, which flows parallel to the coast, 10 km upriver from the mouth, causing ponding and local flooding in subsequent rainy seasons (Wright & Mella, 1963). Co-seismic subsidence was estimated around 1.5 m at Queule and is evident in photographs before and after the event (Weischet, 1960, 1963; Figure 2). Likely due to the subsidence, water drainage became poor, and many agricultural fields remained inundated by 0.5–1 m of water for up to a year after the event (Alvarez, 1963; Weischet, 1963; Wright & Mella, 1963; see Tables SI-1 and SI-2).

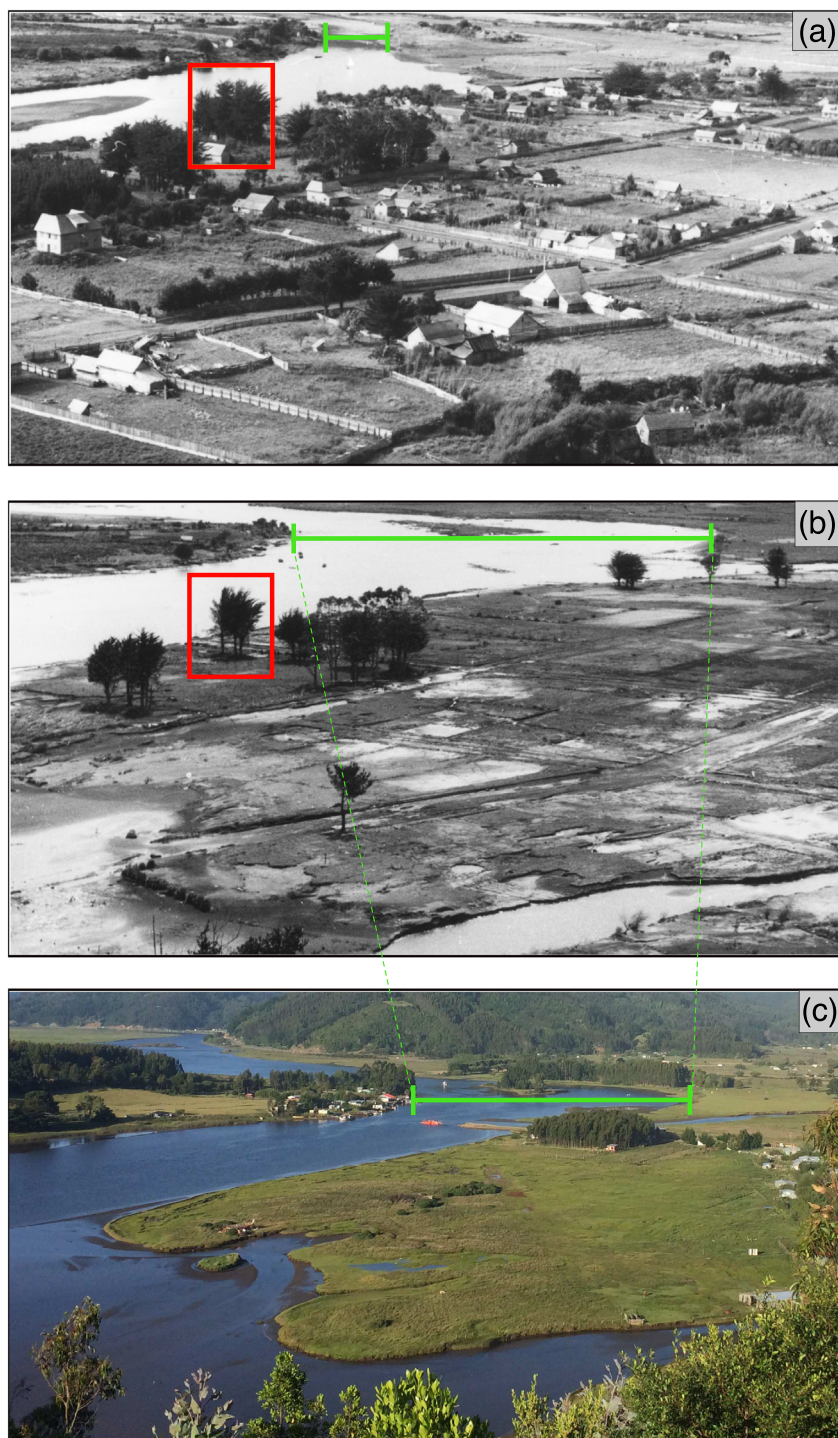


**FIGURE 2** Photographs of Queule town before (a) and after (b) the 1960 earthquake and tsunami from the same location (Weischet, 1963). Bottom photograph (c) was taken from approximately the same angle by Pedro I. Matos-Llavona in January 2018. Green line (a, b) depicts the change in Queule River width before and after the 1960 earthquake. Red square is a reference marker of the same features identified in different photos

At other sites in the vicinity of Queule, the second wave was also destructive at Toltén, 20 km to the north (Alvarez, 1963). In Mehuín, 4 km south of Queule, the third wave was the largest, with an estimated wave height of 7–8.5 m above ground (Sievers et al., 1963; Weischet, 1963; Wright & Mella, 1963).

## 2 | METHODS

### 2.1 | Mapping, stratigraphy, sedimentology, and chronology

The 1960 sandy tsunami deposits are delineated by the high-reflectance areas in a 1961 aerial photograph (see Figure SI-1 in the online

Supporting Information; OEA-Chile, 1961–1962). Darker patches with lower reflectance were interpreted as bare ground without tsunami sand, thickly vegetated areas, or water bodies. Inland areas where the reflectance is diffuse were mapped as possible 1960 tsunami deposits.

We made stratigraphic descriptions from 111 hand-excavated pits, transects of gouge cores, and cut-banks along drainage ditches and rivers in January 2018 and 2019. We described stratigraphic layer thickness, contacts between layers, sedimentary structures, color, sediment texture, and organic composition using the methods of Troels-Smith (1955) (Nelson, 2015). Subsurface sediment samples were collected in 1 inch-diameter cores, box monoliths, and bags. Cores and box monoliths were sampled in the laboratory for grain-size analysis and plant macrofossils for radiocarbon dating (e.g. Kemp et al., 2013).

Our identification criteria for tsunami deposits were: (1) sand layers with a sharp basal contact (<1 mm) above organic-rich soils marking former marshes and pastures; and (2) laterally extensive sand layers that gradually thin inland across the study area (Atwater & Hemphill-Haley, 1997; Bourgeois, 2009; Cisternas et al., 2005; Minoura & Nakaya, 1991; Moore et al., 2007; Morton et al., 2007; Nelson et al., 1996; Peters & Jaffe, 2010; Shennan et al., 2016).

We measured deposit thickness and collected sediment samples from the 1960 tsunami deposit and older sand layers along multiple transects trending landward, perpendicular to the coast, using 2.5 cm-diameter gouge cores. We sampled the 1960 and older buried sand deposits at depth intervals of 2–5 cm, depending on the bed thickness, to analyse spatial and temporal changes in grain-size distribution. For sand units thinner than 2 cm, we collected one representative sample. Box monoliths (40.5 cm long, 9 cm wide, and 3 cm thick) were collected from the exposed stratigraphy for further sampling in the laboratory. We also sampled sediments from the neighboring beach in the swash zone and from eolian dunes.

We used a differential global positional system (GPS base station unit coupled with a floating tide gauge and a pressure sensor deployed for 1.5 days to measure the water level in the tidal channel near Nigue Sur (Figure 1). The water-level measurements were compared to the global tidal model TPX08-atlas, version 1, to obtain mean sea level (MSL) datum within  $\pm 8.1$  cm at one standard deviation (Egbert & Erofeeva, 2002; Ely et al., 2014). To measure the elevations of our stratigraphic cores and pits, we used a land-survey level and measuring rod from an established on-site benchmark referenced to the differential GPS base station.

Organic material was removed with 30% hydrogen peroxide treatment, and the fine-sediment particles were disaggregated by adding sodium hexametaphosphate and applying ultrasound. Grain size was measured using the Mastersizer 3000<sup>®</sup> laser diffraction particle-size analyser with a large-volume, automated, wet-sample dispersion unit.

AMS radiocarbon ages were used to estimate the ages of tsunami deposits. In the laboratory, muddy organic-rich sediment above and below tsunami sand layers in the box monoliths were sliced vertically, viewed under the microscope, and datable organic material was extracted (e.g. Kemp et al., 2013). Fourteen detrital samples from below and above the tsunami sands were submitted for radiocarbon dating (Table 2). The samples with the youngest ages below each of the buried candidates for tsunami sand layers in a continuous stratigraphic sequence were selected as the best estimates of the maximum ages of the sand deposits (Nelson et al., 2021).

## 2.2 | Tsunami numerical simulations

A digital terrain model (DTM) was purchased from a Chilean company (Integral Computing – Geographic Information Systems), who produced a surface model with 5 m horizontal resolution derived from LiDAR measurements referenced to EGM08 datum, which is  $0.0 \pm 0.25$  cm from MSL. During the 1960 tsunami, the sand dunes were eroded by an unknown amount; however, we assume that our model is an adequate representation of the 1960 topography because eolian processes have rebuilt at least some of the dune height in subsequent years based on eyewitness interviews (Table SI-1). The bathymetry used was the General Bathymetric Chart of the Oceans

(GEBCO) with 30 arc-sec resolution. We resampled the bathymetric data to a 5 m grid and merged it with the corrected 5 m DTM to create a final digital surface ( $9.8 \times 5.3$  km) that we used as input for the numerical simulation.

To estimate wave height and inundation extent, we used the GeoClaw forward tsunami hydrodynamic model version 5.7.1 (Bale et al., 2003; Clawpack Development Team, 2017; Leveque et al., 2011). This model solves nonlinear two-dimensional shallow-water equations using a finite-difference numerical scheme with an adaptive mesh refinement (AMR) (Leveque et al., 2011). The GeoClaw model complies with the National Tsunami Hazard Mitigation Program (NTHMP) tsunami benchmark standards and has undergone verification and validation tests (Arcos & LeVeque, 2015; González et al., 2011; Synolakis et al., 2008). As inputs to GeoClaw, we used the digital surface described above as well as three earthquake source models with a Manning's bottom roughness coefficient of 0.025.

We considered three sources in order to determine whether and where the simulated 1960 tsunami would overtop the coastal sand ridge, and if they would correspond to eyewitness observations. Using three sources would reduce uncertainty on specific site sensitivity to different seafloor deformation (see Figure SI-2). Barrientos and Ward (1990) developed a variable slip rupture inversion based on co-seismic land-level change measurements (Plafker & Savage, 1970) and a planar fault geometry. Moreno et al. (2009) proposed a model derived from the same measurements of co-seismic land-level change, but used a non-planar three-dimensional fault geometry determined from multiple types of geophysical data. Dolcimascolo (2019) developed a model derived from a suite of probable earthquake sources constrained by 19 tsunami wave-height observations compared to 30 computed tide gauges and 11 tsunami deposit locations. Out of 423 earthquake rupture scenarios with different slip distributions, the source '40\_93\_2' from Dolcimascolo (2019) was the scenario that best fit the 1960 tsunami observations at multiple sites along the coast.

## 3 | RESULTS

### 3.1 | Numerical simulations of the 1960 tsunami

The simulations of the 1960 tsunami correlate well with evidence from primary sources, including historical reports, eyewitness interviews, and 1961 aerial photographs, that confirm the widespread effects of the 1960 earthquake and tsunami in the Queule region (Weischet, 1960, 1963; Tables SI-1 and SI-2; Figures SI-1 and SI-3). All three simulation sources resulted in tsunami inundation up to 3.5 km inland in the lower Queule River valley and tributaries (Figure 3). The coastal sand dunes were overtopped, and modeled inundation submerged all the sites where the 1960 tsunami deposit was observed (Figure 3). The inundation extent closely followed the topography, reaching the steeper hillslopes on the eastern edge of the Queule valley. The steep valley slopes created conditions that produced edge waves and significant tsunami wave reflection, causing complex hydrodynamic interactions with incoming waves. The high eolianite hill at the southern end of the Queule peninsula (Figures 1b and 3b) was the only coastline feature that remained above water, which is consistent with witnesses' observations (Table SI-1). Maximum wave heights near the shoreline (Gauge #33 in Figure 3) ranged

from 10.5 to 12.0 m. The sources of Barrientos and Ward (1990) and Dolcimascolo (2019) predicted the second wave to be the highest, at 11.5 and 10.5 m, respectively, whereas the first wave was highest, at 12.0 m, using the Moreno et al. (2009) source. By the third wave, all simulations show significantly smaller wave heights (Figure 3c).

At inland locations along the Queule River, maximum simulated wave heights ranged from 7.2 to 10.2 m above MSL (Table 1). These are greater than the historical estimate of the minimum wave height of 4–4.5 m above ground measured from the debris in trees 1.5 km inland from the coast (Weischet, 1960, 1963). However, given the range of ground-surface elevations from 0.2–4.2 m above MSL at the potential locations of the trees harboring the tsunami debris, and that the debris represents a minimum flow depth and the simulations a maximum wave height, the two sources of information are not necessarily contradictory. The simulations show an extended duration of inundation, with later waves propagating over previously flooded

areas, demonstrating poor sea-water drainage as confirmed by eyewitness accounts and written reports (Weischet, 1963; Wright & Mella, 1963; Tables SI-1 and SI-2).

### 3.2 | Stratigraphy

The well-preserved stratigraphy at Nigue Sur displays three distinct stratigraphic zones: Stratigraphic Zone #1 contains the 1960 tsunami deposit and two sand layers that may be older tsunami deposits; Stratigraphic Zones #2 (alternating silt and peat layers) and #3 (basal sand) are included to provide context and contrast with Zone #1, which is the main focus of this study. Portions of the three stratigraphic zones were found in other locations within the Queule study area, indicating that this general stratigraphy is widespread.

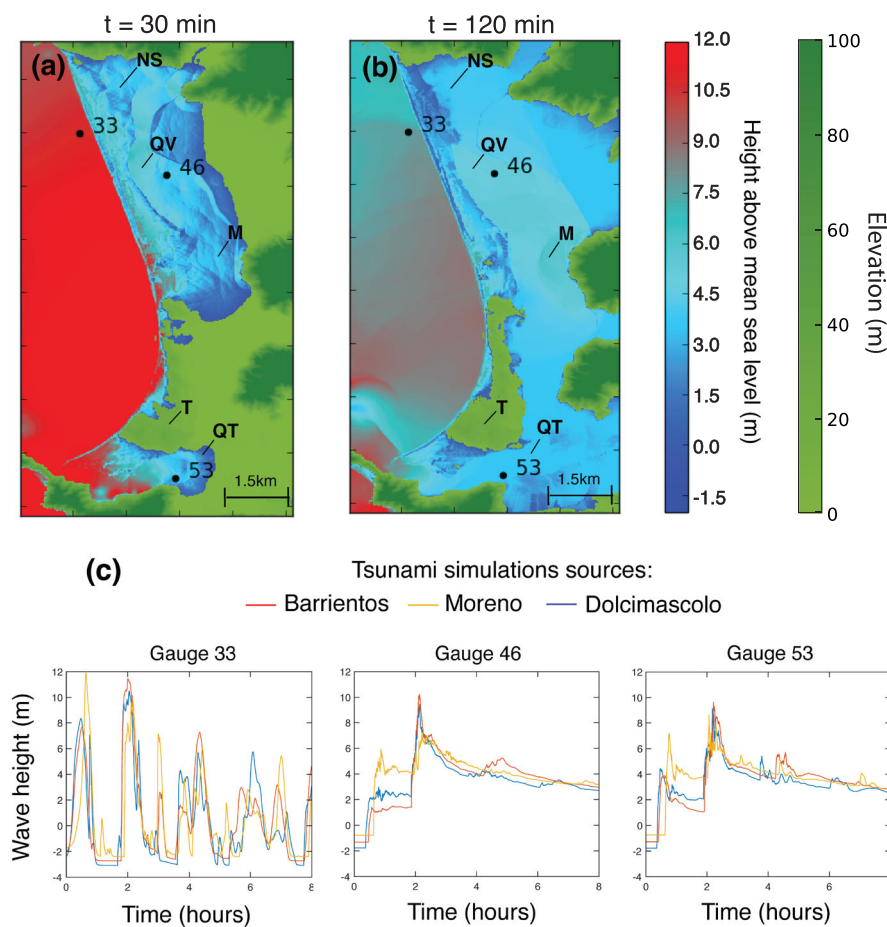


**FIGURE 3** Snapshots of GeoClaw simulation results showing inundation and wave height of the 1960 tsunami using the earthquake rupture source from Moreno et al. (2009). The snapshots show the first wave inundation at 30 min (a) and near the time of maximum inundation by the second wave at 2 h (b). The numbers represent the synthetic tide gauge locations. The letters depict the following locations: Nigue Sur (NS), Queule Victoria (QV), Maitenco (M), and Queule town (QT) (Figure 2). (c) Synthetic tide gauge waveform showing a time series of water height during the 1960 tsunami simulation at three synthetic tide gauges from three earthquake source models: Barrientos and Ward (1990) in red; Moreno et al. (2009) in yellow; and Dolcimascolo (2019) in blue

**TABLE 1** GeoClaw forward tsunami simulation results from three earthquake sources

Item description	Barrientos and Ward (1990)	Moreno et al. (2009)	40_93_2 (Dolcimascolo, 2019)	Average
Max. wave height at shoreline (Gauge #33) (m)	11.5	12.0	10.5	11.3
Max. wave height near Nigue Sur and Queule Victoria (Gauge #46) (m)	10.2	7.2	9.4	8.9
Max. wave height near Queule town (Gauge #53) (m)	9.7	8.7	9.14	9.16
Historical flow depth approximation near Queule town (m) <sup>a</sup>	n/a	n/a	n/a	>4–4.5
Arrival order of highest wave at shoreline	2nd	1st	2nd	n/a

<sup>a</sup>As described by Weischet (1963).

3.2.1 | 1960 Tsunami deposit

The 1960 tsunami sand deposit can clearly be identified in 1961 aerial photographs. The maximum distance is 2.2 km inland at the southern end of the study area near the Queule River inlet and 1.3 km inland at the northern end of the study area (Figures 4 and SI-1). We verified the extent of the sand deposit on both sides of the river. Eyewitness accounts confirm that sand blanketed the landscape inland (east) of the Queule River (Table SI-1; Wright & Mella, 1963). The locations near the dunes with the highest image reflectance in the 1961 aerial photographs corresponded to a thicker 1960 tsunami deposit. Our field measurements show that the sand deposit generally thinned landward from a maximum thickness of 122 cm near the coastal dunes at Nigue Sur to <1 cm thick 800 m landward from the shoreline (Figure 4).

At Nigue Sur (Figure 1), the 1960 sand deposit is tabular, laterally extensive, and generally massive (Figure 4). Where we measured vertical grain-size distribution (Figures 4C-C', the sand unit exhibits cycles of normal and reversed grading. Mud rip-up clasts were observed within the deposit in several pits. The lower contact is sharp and irregular, where sand fills depressions or post-depositional bioturbation burrows. In contrast, the upper contact is gradational, with the overlying soil A horizon in most pits and cores.

The 1960 sand layer along the Queule Victoria transect (Figures 4 and SI-4, SI-5) is generally massive, with a few sections of normal grading. The median grain size and thickness of the deposit show a general landward decrease (Figure 4C-C'). Isolated thick patches of 1960 tsunami sand form minor hummocky peaks in the modern surface topography.

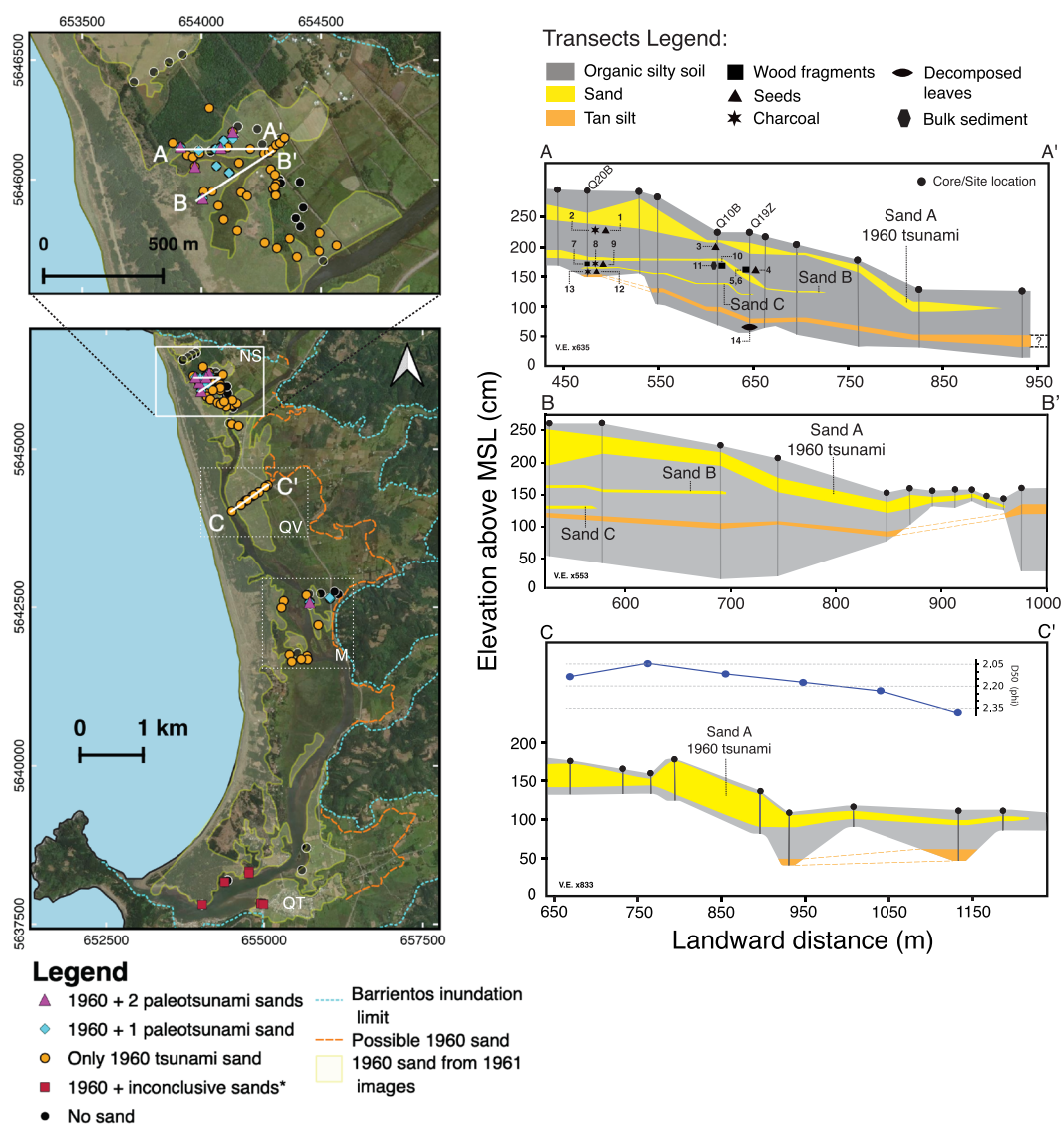


**FIGURE 4** Map showing tsunami deposits and simulated inundation near Queule. The extent of the 1960 tsunami sand deposit is based on 1961 aerial imagery. Shaded yellow polygon = high reflectance of 1960 sand; dashed orange line = diffuse reflectance of possible 1960 sand. The inundation extent of the 1960 tsunami GeoClaw simulation is shown by the blue dashed line. The presence or absence of deposits from the 1960 tsunami and two paleotsunami deposits in cores and pits are indicated by dots, diamonds, and triangles. Stratigraphic profiles along transects A-A', B-B', and C-C' are in boxes at right. Sand A is the 1960 tsunami deposit and sands B and C are interpreted as paleotsunami deposits. Vertically averaged  $D_{50}$  median grain size of the 1960 tsunami deposit is shown in blue at the top of box C-C'. Dashed outline boxes represent the locations Nigue Sur (NS), Queula Victoria (QV), Maitenco (M), and Queule town (QT)

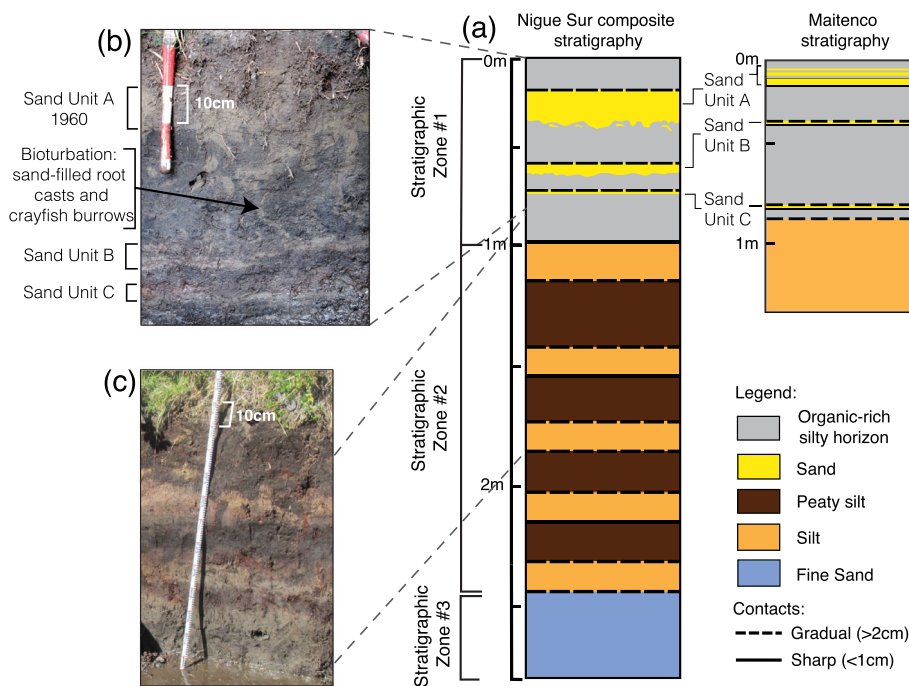


**FIGURE 5** Nigue Sur and Maitenco site composite stratigraphy. (a) Three distinct sedimentary environments divided into Stratigraphic Zones #1, #2, and #3. This study focuses on the stratigraphy and sand layers in Stratigraphic Zone #1 in the upper 1 m. (b) Photograph of site Q20B showing the three tsunami sand layers and bioturbation features from root casts and shrimp burrows. (c) Photograph of Stratigraphic Zone #2 in a drainage ditch. Light layers are inorganic silt, dark layers are peaty silt

The characteristics of the 1960 tsunami deposit at the Maitenco site (Figures 1 and 5) are similar to those in Nigue Sur: laterally extensive, medium to fine sand with a sharp (<1 mm) lower contact and low organic content. A series of fine sand–silt couplets overlie the 1960 tsunami sand deposit in exposures along the Queule riverbank at Maitenco (Figure 5). Within a 20 cm-thick sequence of couplets (6–26 cm), the couplet thickness decreases from 6 to 2 cm with a total of four couplets.

A low-elevation cut-bank outcrop across a narrow stream near Queule town contains multiple sand layers in the upper 50–70 cm that did not exhibit lateral continuity or the consistent stratigraphic pattern of the other study sites. One or more of these sand layers is likely the 1960 tsunami deposit. Overlying the sand layers is 20 cm of fine sand–silt couplets that decrease in thickness upwards in the outcrop, similar to those observed at Maitenco (Figure 5). An ~1 cm-thick sand below the modern grass roots was interpreted as deposited by the 2010 Maule Chile tsunami (Fritz et al., 2011). The 2010 tsunami inundated this site, and sand deposits from that event were observed shortly afterwards on the ground surface (Eduardo Jaramillo, Universidad Austral de Chile, oral communication, 2018).

### 3.2.2 | Stratigraphic Zone #1: Paleotsunami deposits

Stratigraphic Zone #1, in the upper ~90 cm at the Nigue Sur and Maitenco sites (Figure 1), consists of dark brown to black, sandy organic silt layers with three interbedded, laterally continuous sand layers: sand A (the 1960 tsunami sand), and similar sands B and C, interpreted as paleotsunami deposits (Figures 4 and 5). The dominant components of the stratigraphy between the sand layers in Zone #1 are silt (25–75%) and organic humus (25–50%), with <12% sand. Depending on the location, the fraction of highly decomposed organic material is up to 75%. There are no distinct, visible differences in the organic content, grain size, or color of the organic-rich layers directly below and above each sand layer.

Sand B is generally tabular and extends up to ~250 m inland. It is thickest at sites close to the coastal dunes (~10 cm), and retains a consistent thickness of ~2 cm up to 250 m inland from the dunes at Nigue Sur (Figure 4). It is an average depth of 56 cm below the modern surface and 20 cm below sand A (Figures 4 and 5B). Sand B is composed of inorganic, medium to fine, well-sorted, sub-rounded grey sand. Oxidation staining is minimal relative to sand A. Sand B has sharp (<1 mm) lower contacts, which are often irregular.

Sand C is consistently 1–2 cm thick, with an average depth of 1 m. It extends up to 200 m inland from the coastal dunes at Nigue Sur (Figure 4). Sand C is slightly finer grained than sand B, and composed of fine, well-sorted, subrounded, grey sand (see Figures SI-4 and SI-5). The lower contact is sharp (<1 mm).

Vertical structures suggesting bioturbation were observed in sands A, B, and C. A conspicuous example is sand A in a forested area (Figures 5b and SI-6). Here, the 1960 tsunami sand filled 1–2 cm-thick root casts and freshwater crayfish burrows underlying the sand layer. Sand A also shows structures that we infer to record trampling, especially on seasonally saturated marsh or pasture soils. Trampling pushed the sand downwards to a greater depth than the average level of the sand A bed; in some cases, short sections of the depressed sand layer remain horizontal. We observed this process in modern wetland soils where present-day animal grazing deforms the surface up to ~30 cm.

The modern processes of bioturbation of the 1960 sand A were used to interpret similar features commonly observed in the older sand layers throughout the Nigue Sur site, especially in sand B. Bioturbation caused local disruptions in the lateral continuity of sands B and C. At some locations, additional sand layers similar to sands B and C were observed at multiple depths in gouge cores. However, after comparing the cores to the wider exposure of the stratigraphy in excavated pits at the same locations, we concluded that these apparent lower sand layers were in fact sand lenses produced by bioturbation. For example, Figure 5b shows how burrows filled with sand from an overlying tsunami deposit can result in a duplicate sand lens up to 50 cm below the original deposit.



The Maitenco site (Figure 4) also contains three sand deposits interbedded with organic-rich silt overlying a tan inorganic silt layer. These layers together are similar in stratigraphic position, sediment and organic composition, and thickness to the 1960 sand A and sands B and C in Zone #1 at Nigue Sur, as well as the uppermost tan silt layer in Stratigraphic Zone #2.

### 3.2.3 | Stratigraphic Zone #2: Silt and peat layers

Stratigraphic Zone #2 consists of four repeated sequences of silty peat layers interbedded with layers of inorganic silt (Figure 5). All layers are laterally continuous for at least 400 m across the Nigue Sur site, exposed by freshly excavated drainage trenches (>1 km long and ~2 m deep). Some of the lower contacts are sharp (<1 mm), whereas others are very gradual (<1 cm to >2 mm). The silty peat layers contain 25–50% moderately decomposed organic detritus. The upper two inorganic silt layers are tan, and the lower two are greenish grey. The prominent uppermost tan silt layer in Zone #2 (Figure 5) is consistently encountered in pits across at least 5 km of the northern portion of the Queule study area, including Nigue Sur, Queule Victoria, and Maitenco (Figures 1 and 4). This thick, tan silt forms a distinct contrast with the overlying organic-rich silt and sand layers of Zone #1.

### 3.2.4 | Stratigraphic Zone #3: Basal sand

The lowest described stratigraphic zone is a bluish grey, very fine to fine sand with no observable organic material. The upper contact of this sand is at depths of 2–2.4 m. We were unable to excavate or recover samples below this level because of groundwater saturation and sand infilling the core holes. This thick basal sand was encountered in pits and cores in nearly all parts of the study area, covering a north–south distance of over 5 km.

## 3.3 | Radiocarbon ages

Below sand A, two detrital samples of seed skins and one of charcoal fragments yielded ages of 460–310 cal BP, post-modern (i.e. after 1950 CE) and 530–310 cal BP, respectively (Table 2; Figure 6). The maximum limiting age of 1950 CE supports the interpretation that sand A is the 1960 tsunami deposit. The two samples with ages greater than 300 years suggest either that detrital plant fragments have a residence time of a few hundred years near the surface in this environment, or that they represent older organics from a newly exposed surface following tsunami wave erosion.

Radiocarbon ages from seeds, wood fragments, and charcoal from the upper portions of the stratigraphy underlying sands B and C were used to constrain the maximum age of these sand deposits. We used the youngest radiocarbon age associated with each sand layer as a maximum limiting age of the sand deposition: 4960–4520 cal BP for sand B and 5930–5740 for sand C. However, future analysis of additional samples could refine the large range in the radiocarbon ages below sand B (~1000 years) and potentially increase the best-fit age for sand B.

Very dark, slightly decomposed leaves 1 cm below the uppermost tan silt layer in Stratigraphic Zone #2 yielded an age of 6290–6000 cal BP (Table 2, Figure 5), which is consistent with its stratigraphic position underlying the samples from Zone #1.

## 4 | DISCUSSION

### 4.1 | 1960 Tsunami deposit and co-seismic land deformation

We infer that the shallow, thick, widespread deposit throughout the Queule region (sand A) is the deposit of the 1960 tsunami. We base

**TABLE 2** Radiocarbon ages from the Nigue Sur site. All samples were measured with accelerated mass spectroscopy (AMS) at the National Ocean Sciences Accelerator Mass Spectrometry (NOSAMS) facility. The ages were calibrated with the southern hemisphere radiocarbon calibration curve (SHCal20) with the Bayesian age model OxCal v4.4 (Bronk Ramsey, 2009; Hogg et al., 2020) and presented as calibrated ages before 1950 (cal BP)

Sample id	Site id	Lab id	Description and stratigraphic layer	Depth (cm)	Calibrated 2 $\sigma$ age range (cal BP)	Conventional $^{14}\text{C}$ age
1	Q20B	OS-148342	Seed coatings below sand A	35	460–310	365 $\pm$ 15
2	Q20B	OS-148313	Charcoal fragments below sand A	35	530–310	435 $\pm$ 60
3	Q10B	OS-148367	Seed coatings below sand A	13	After 1950 CE	Post-Modern
4	Q19Z	OS-144128	Seed samples above sand B	62 <sup>a</sup>	1280–950	1230 $\pm$ 75
5	Q19Z	OS-144129	Wood fragments above sand B	62 <sup>a</sup>	4580–3640	3790 $\pm$ 160
6	Q19Z	OS-142026	Wood fragments above sand B	82 <sup>a</sup>	630–320	505 $\pm$ 70
7	Q20B	OS-147375	Wood fragments below sand B	77	5590–5320	4780 $\pm$ 30
8	Q20B	OS-147450	Charcoal below sand B	68	5310–5040	4550 $\pm$ 25
9	Q20B	OS-147504	Seeds and seed coatings below sand B	77	5750–5470	4920 $\pm$ 55
10	Q10B	OS-142025	Wood fragments below sand B	38	4960–4520	4250 $\pm$ 70
11	Q10B	OS-142054	Bulk sediment sample below sand B	35	1370–1300	1500 $\pm$ 15
12	Q20B	OS-147451	Seeds and seed coatings below sand C	99	6180–5900	5240 $\pm$ 30
13	Q20B	OS-147376	Charcoal below sand C	87	5930–5740	5140 $\pm$ 30
14	Q19B	OS-142056	Leaves below uppermost silt layer	131	6290–6000	5410 $\pm$ 25

Note: Samples were sent to the Woods Hole Oceanographic Institution NOSAMS laboratory for analysis of radiocarbon isotope  $^{14}\text{C}$  with AMS.

<sup>a</sup>Stratigraphic position between sand layers A and B.

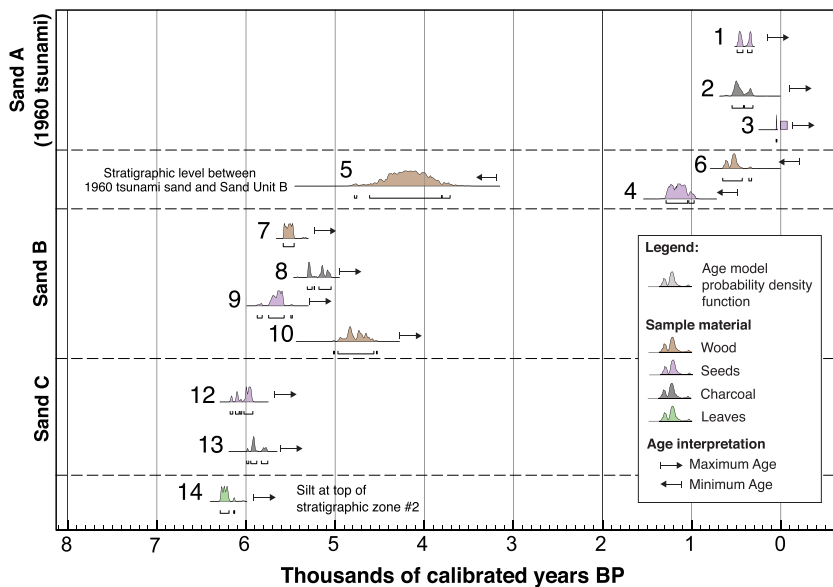


**FIGURE 6** Compilation of radiocarbon age results at the Nigue Sur site. Samples were collected 0–1 cm below each sand layer except samples 4 and 5, which were sampled between sand B and the 1960 sand. No vertical scale; probability density functions of ages are not arranged by stratigraphic position. Calibration was made using OxCal<sup>®</sup> v4.4 southern hemisphere radiocarbon calibration curve SHCal20 (Bronk Ramsey, 2009; Hogg et al., 2020)

our interpretation on the common characteristics the deposit shares with other published descriptions of tsunami deposits (e.g. Morton et al., 2007), on the consistency of the observed deposit extent with eyewitness accounts and with aerial photographs from 1961, and on the agreement between the predictions of our numerical simulations and witness reports.

Evidence of co-seismic subsidence during the 1960 earthquake has persisted for years to decades. The Queule River remains wider today than before the earthquake. The sand–silt couplets overlying the 1960 tsunami deposits at Queule town and Maitenco are interpreted as intertidal sediments reworked and deposited by the highest tides following co-seismic land-level subsidence. Similar deposits were documented in Alaska after the 1964 earthquake (Atwater et al., 2001).

## 4.2 | Paleotsunami deposits

We interpret as paleotsunami deposits two additional sand layers (sands B and C) with maximum ages of 4960–4520 and 5930–5740 cal BP, respectively. These two sand layers are also composed of well-sorted, inorganic sand, are tabular, and have sharp lower contacts. Although they display local discontinuities due to bioturbation by trampling and burrowing, all three tsunami sands are laterally extensive across multiple sites over 200 m inland of the coastal sand ridge (Figure 4). Storm surges or wind are other possible sediment sources for sands B and C. However, deposits from tsunamis are the most likely to maintain such consistent stratigraphic characteristics over a broad area. For example, the Nigue Sur and Maitenco sites are over 4 km apart and occupy different positions relative to the river, coast, and sand ridge, yet exhibit remarkably similar stratigraphy (Figure 4).

The stratigraphy of the low-elevation sites near the town of Queule contained multiple sand lenses, possibly due to greater interaction with the river and tidal processes and disturbance by human activity. This stratigraphy could not be correlated with the other, more protected and well-preserved sites.

## 4.3 | A gap in the tsunami record

If, as we infer, sands B and C are tsunami deposits similar to the 1960 sand deposit, we are faced with a problem: a 4500-year gap in the stratigraphic record in which no other tsunami deposits are preserved. For example, if the 1575 event was similar in size and extent to the one in 1960, as indicated by evidence at other places along the south-central coast of Chile (Atwater et al., 2013; Cisternas et al., 2005; Cisternas, Carvajal, et al., 2017; Cisternas, Garrett, et al., 2017; Ely et al., 2014), why are there no 1575 tsunami deposits in Queule, although it is located midway between those other places? Possible explanations could include: (1) the 1960 tsunami was particularly large at Queule, exceeding the size of historical tsunamis in the last 500 years or even longer at this site; (2) co-seismic subsidence in 1960 was greater than in previous events; (3) the coastal geomorphology and relative sea level have changed, precluding deposition and/or preservation of tsunami deposits between ~4500 BP and 1960 CE; or (4) tsunami deposits between ~4500 BP and 1960 CE have been selectively eroded or destroyed. We discuss these different possibilities in terms of our field evidence and modeling results and their implications for the megathrust earthquake history of south-central Chile.

## 4.4 | Comparing the 1960 tsunami to the historical record

Absent from Queule is evidence of at least three historically documented large subduction-zone earthquakes and/or tsunamis in the last 500 years, in 1575, 1737, and 1837 (Figure 1; Cisternas et al., 2017a). Previous paleoseismic studies interpreted tsunami deposits from the 1575 tsunami at both northern sites in Tirúa (Dura et al., 2017; Ely et al., 2014) and southern sites in Maullín (Cisternas et al., 2005), Chucalén (Garrett et al., 2015), Cocotué (Cisternas, Garrett, et al., 2017), Chaihuín (Aedo et al., 2021; Hocking et al., 2021), and Lakes Huelde and Cucao (Kempf et al., 2017, 2020) (sites located in Figure 1). Historical and geological evidence of the

1837 earthquake indicate a smaller size than in 1575 and 1960, and the rupture was likely in the southern portion of the 1960 rupture zone (Cisternas, Carvajal, et al., 2017). A deposit interpreted as the 1737 tsunami is present at Chaihuín (Aedo et al., 2021; Hocking et al., 2021), 70 km south of Queule, but has not been identified in other historical or geological records in Chile.

Based on the evidence of these previous earthquakes and tsunamis at other sites, along with the geomorphic setting and geographic location of the Queule site, we expected to find a deposit from the 1575 tsunami and potentially from 1737 or 1837. We found no deposits from any of these historic events. If the geometry of the coast and dune ridge was the same as today, our evidence would indicate that these historical tsunamis were not capable of producing deposits similar to those of the 1960 tsunami at Queule.

Another possibility is that the specific rupture pattern of the 1960 earthquake was conducive to generating a particularly large tsunami at the Queule site. All crustal deformation inversion studies

show the maximum slip of the 1960 rupture close to the latitude of Queule (Barrientos & Ward, 1990; Fujii & Satake, 2013; Moreno et al., 2009), potentially making the tsunami especially large at this site. This scenario does not necessarily suggest that the 1960 earthquake was larger overall than in 1575, but rather that the tsunami produced by the 1960 rupture exceeded the tsunamis produced by the 1575 and 1837 earthquake ruptures at this location, if no major changes in geometry and sand source occurred during the intervening time period.

Earlier, smaller tsunamis could have travelled up the Queule River without overtopping the dunes, inundating the landscape without transporting a sufficient amount of sand-sized sediment to leave a thick sand deposit that would be preserved in the stratigraphic record. It would be expected that the 1837 tsunami did not leave geologic evidence because the latitudinal extent based on historical records locates this event farther south in the subduction zone (Cisternas, Carvajal, et al., 2017). However, in two independent interviews, local

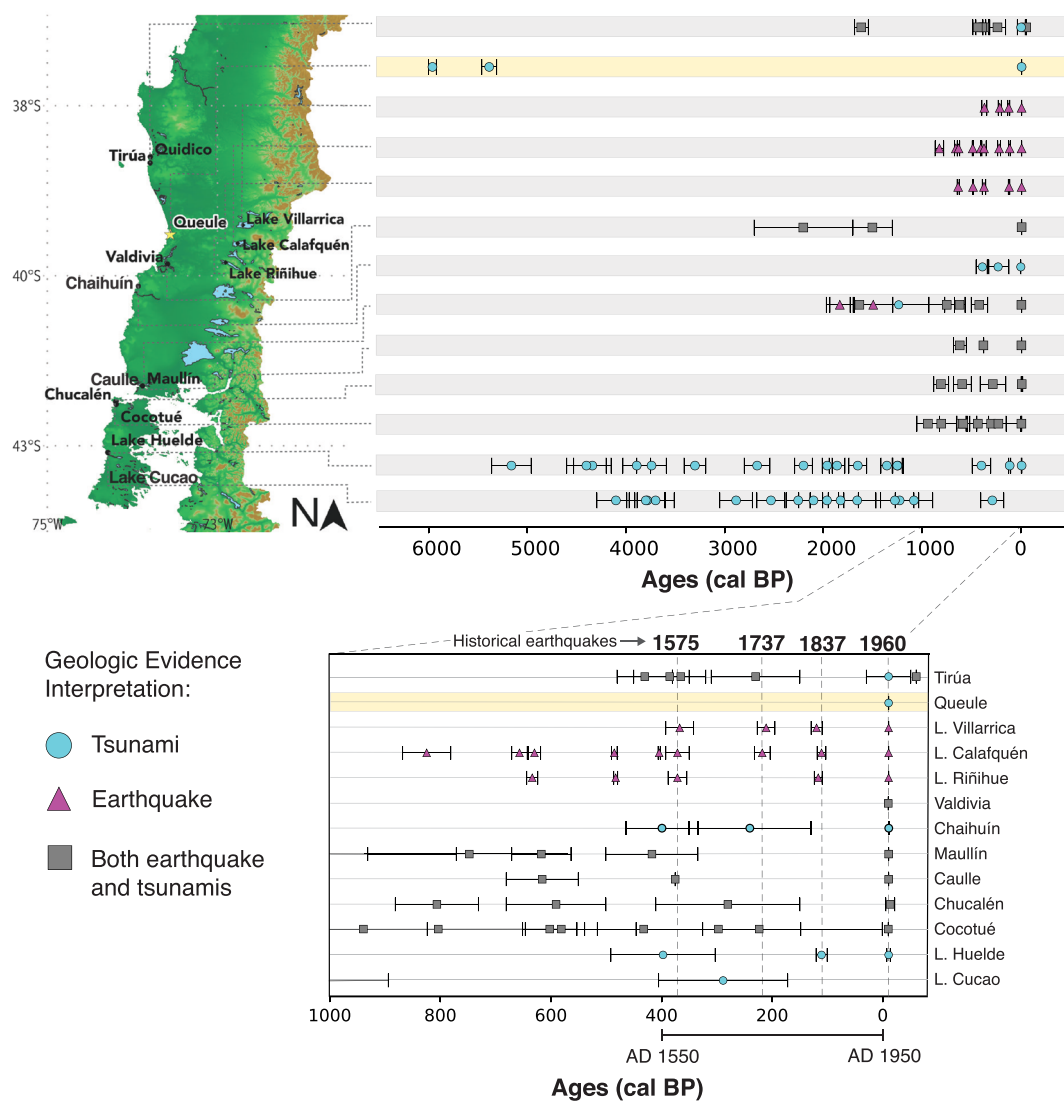


**FIGURE 7** Ages for paleoseismic events in south-central Chile with  $2\sigma$  probability ranges. Tsunami-only proxies are tsunami sand deposits in coastal lakes and marshes. Earthquake-only proxies are turbidite deposits in Andean lakes, and co-seismic subsidence in coastal sites. Proxies of both earthquakes and tsunamis are based on coastal stratigraphy where co-seismic subsidence evidence is found along with tsunami deposits. The lower plot shows the past 1000 years and includes the historical earthquakes in south-central Chile: 1575, 1737, 1837, and 1960 (Aedo et al., 2021; Cisternas et al., 2005; Cisternas, Carvajal, et al., 2017; Cisternas, Garrett, et al., 2017; Dura et al., 2015, 2017; Ely et al., 2014; Garrett et al., 2015; Hocking et al., 2021; Hong et al., 2017; Kempf et al., 2015, 2017, 2020; Moernaut et al., 2014, 2018)

residents mentioned a possible historical tsunami before 1960. One of the interviewed residents affirmed that her great-great-grandmother survived an earlier event as a child when 'the sea came out to the land' (Table SI-1). In the other interview, a survivor of the 1960 tsunami mentioned that his great-grandmother witnessed a time when the 'sea overflowed' (Table SI-1). If these oral accounts were passed through three or four generations, they could match the time of the 1837 historical tsunami.

A final factor to consider is possible erosion or lack of preservation of earlier historical tsunami deposits. A 1575 tsunami sand layer near the surface could have been eroded by the 1960 tsunami. Tsunamis that inundated only the low-lying areas near the Queule River might have left deposits that were subsequently eroded by lateral migration of the river, as we found only the 1960 sand overlying mixed fine sediment with no laterally continuous stratigraphic layers in cores close to the river (Figure 4). Farther north in south-central Chile, agricultural furrows have been described in archaeological sites as early as 1200 CE (Dillehay et al., 2007), although no direct evidence has been observed near Queule. A 1575 tsunami sand layer could have been ploughed under, after ploughs were introduced by the Spanish in the mid-16th century. However, if the 1575 tsunami deposited an amount of sand similar to that in 1960 into agricultural fields that were later ploughed, we would expect a higher sand component in the texture of the pre-1960 soil, which is not consistent with our observations. In addition, we found sands A, B, and C across different environments, from forest (Figure 5B) to agricultural pastures.

The presence of sands B and C at multiple sites, with no evidence of another sand layer between these deposits and the 1960 sand at any of our exploratory cores and excavations, makes deposition and selective erosion of earlier historical tsunami deposits unlikely. Geological evidence from other sites in coastal Chile indicates multiple tsunamis of magnitude similar to the 1575 tsunami over the last few thousand years (Figure 7). If the 1575 tsunami left a deposit that was later eroded, we would expect to find evidence of deposits from some of these older events in the underlying undisturbed stratigraphy above sand B. Whether the historical tsunamis left deposits at Queule, the broader question remains the explanation of the >4500-year gap in the paleotsunami record, which is most relevant to the interpretation of stratigraphic preservation of tsunami deposits in other similar geomorphic settings.

#### 4.5 | Stratigraphic records of older tsunamis in south-central Chile

Sand C at Queule extends the tsunami catalogue for southern Chile to 5930–5740 cal BP (Figure 7). The only other tsunami record that approaches the age of the oldest tsunami deposits at Queule is from Lake Huelde, a coastal lake in southern Chiloé Island that has preserved 17 tsunami deposits in the last 5500 years (Kempf et al., 2017; Figure 7). The lowermost and oldest sandy layer at Lake Huelde, hQ (5360–4960 cal BP) is slightly older than the estimated maximum limiting age of sand B at Queule (4960–4520 cal BP) (Figure 7).

The simplest explanation of the tsunami deposit record in Queule would be that the 1960 tsunami was the largest in over 4500 years, and it was the only tsunami capable of overtopping the sand ridge

since the deposition of sand B. That scenario is unlikely, as other paleoseismic records indicate the occurrence of tsunamis and earthquakes over the last 2000 years that could have been similar to the 1960 event in magnitude or extent (Cisternas et al., 2005; Cisternas, Garrett, et al., 2017; Moernaut et al., 2018). However, the sediment cores from Lakes Huelde and Cucao on Chiloé Island indicate that the 1960 tsunami could have been an unusually large event when compared with many others over the last 5000 years (Kempf et al., 2017, 2020). The 1960 deposit is the most widespread deposit at both lakes, although at Lake Cucao it closely resembles the 1575 tsunami deposit. Better preservation of the 1960 deposit is to be expected because it is the most recent. However, several of the more recent deposits in Lake Huelde, including the deposits from 1575, are not as extensive or do not contain as many characteristics diagnostic of large, erosive tsunamis as some of the older layers, so age-biased preservation is not the only factor.

#### 4.6 | Relative sea level and coastal evolution

The long period of >4500 years with no tsunami deposition and/or preservation seems more plausibly explained by changes in coastal geomorphology within the context of RSL variation rather than a complete absence of tsunami occurrence. A possible explanation for the discontinuous record of tsunami deposits at Queule is that the site geomorphology has changed over the last 6000 years, partially in response to the general fall in RSL since the mid-Holocene. Holocene sea level reached an estimated high-stand in south-central Chile of 0.5–8 m above modern mean sea level (a.s.l.) at 8000 or 7000 cal BP, based on glacial isostatic adjustment (GIA) models and relative sea-level index points across south-central Chile (Dura et al., 2016; Garrett et al., 2020). The high-stand lasted ~1000 years, followed by a fall in RSL through the late Holocene (Figure 8). Long gaps in the stratigraphic record have also been observed at other coastal sites in southern Chile, where earthquake and tsunami reconstructions do not pre-date 2000 cal BP, supporting the hypothesis that RSL can affect accommodation space and the creation and preservation of a stratigraphic record (Cisternas et al., 2005; Dura et al., 2016; Garrett et al., 2015; Nelson et al., 2009). Other sites in central Chile show a similar pattern, where six sand beds interpreted as tsunami deposits were found from ~6–3 ka, attributed to a window of RSL rise (Dura et al., 2015).

The stratigraphy at the Nigue Sur site, viewed in the context of RSL history, suggests a rapid rise during the early Holocene, followed by a mid-Holocene sea-level high-stand and a more moderate rate of decline to present sea level during the late Holocene. Under this scenario, we interpret the grey sand in Stratigraphic Zone #3 throughout Queule as having been deposited in an open shallow marine embayment, probably from the early Holocene (Figure 8, Time 1). Stratigraphic Zone #2 represents shallow sub-tidal and tidal marsh sediment older than 6000 years BP, during and immediately after the sea-level high stand (Figure 8; Dura et al., 2016; Garrett et al., 2020). The inorganic silts and interbedded organic-rich silt layers in this zone imply that the Queule sites were in a protected area of quiet water, perhaps a shallow lagoon or an embayment behind a barrier that was farther from shore than today (Figure 8, Time 2). Tsunami sand deposits were not identified in this stratigraphic zone, which suggests

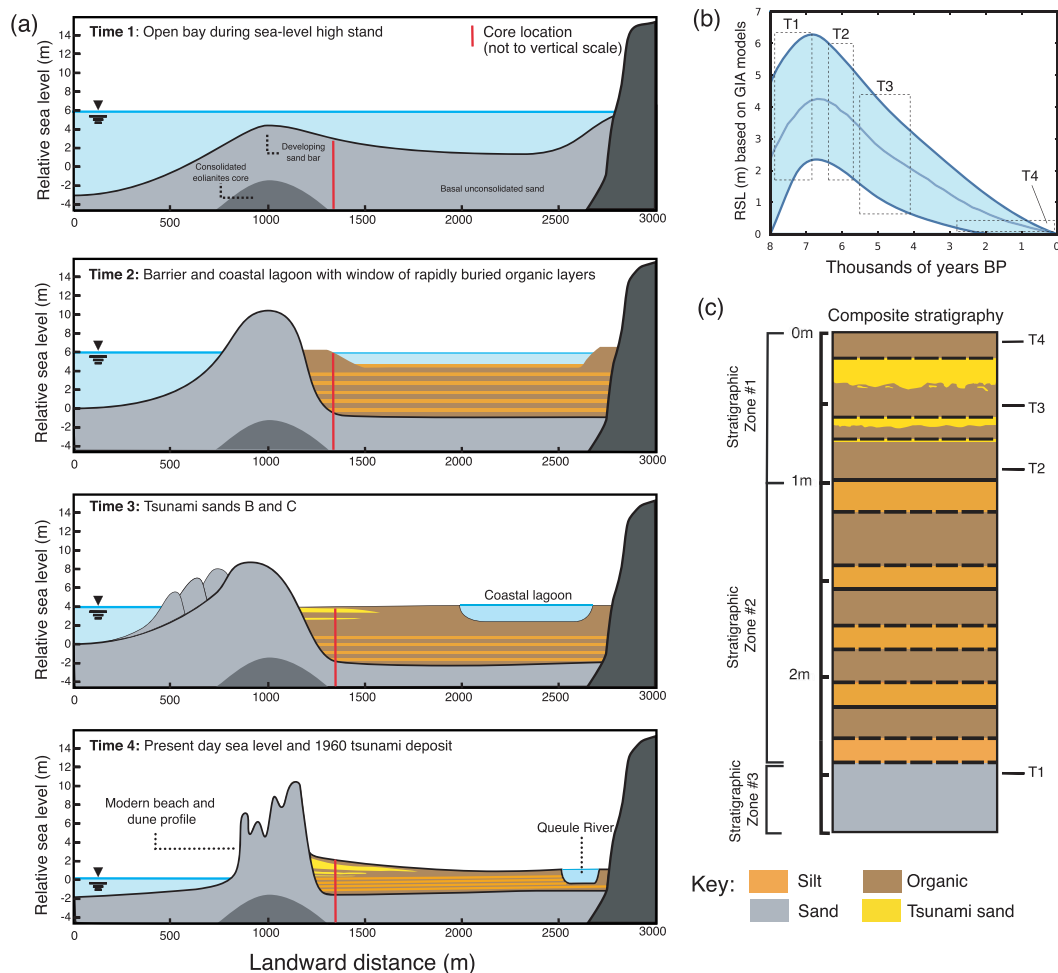


**FIGURE 8** (a) Proposed schematic diagram showing a hypothetical sequence of events that could have led to the formation of the three stratigraphic zones observed in the Queule study sites (Figure 4). The stratigraphic layers are not to scale, except for Time 4 surface only, which depicts a modern elevation profile across Nigue Sur A–A' transect (Figure 4). Time 1: Onset of mid-Holocene high sea-level stand with open bay and deposition of grey sand. Time 2: Latter part of mid-Holocene high stand; alternating inorganic silt and peat layers suggest variations in relative sea level in a shallow lagoon, perhaps representing co-seismic land-level changes. Time 3: Tsunami sands B and C were deposited landward of the sand berm as sea level falls. Time 4: Gradual fall in relative sea level until present day. The 1960 tsunami overtopped the sand barrier, leaving a thick landward sand layer. Migration of the sand barrier between Times 3 and 4 could have resulted in deposition of tsunami sediment farther seaward, thus not preserved landward of the present-day sand spit. (b) Range of relative sea level curves from a suite of glacio-isostatic adjustment models (Garrett et al., 2020). Upper and lower boundaries represent the highest and lowest scenarios, while the middle line represents the mean between these two extreme curves. (c) Composite stratigraphy of Nigue Sur site based on multiple core, pits, trenches, and exposed stratigraphy near Queule (see Figure 5 for details)

that the site was either far from a sand source, meaning the shoreline was seaward of its current position, or that tsunamis were not capable of breaching the barrier that protected the lagoon/marsh site. Analysis of microfossils in these layers would help to reconstruct the depositional environments through time and identify any abrupt changes in RSL that could be associated with seismic land deformation.

As sea level started to fall at  $\sim 6$  ka, the sites preserving sands B and C at Nigue Sur, Maitenco, and probably other locations within the Queule area emerged above sea level. A sand source developed as either the barrier became more exposed or moved inland, closer to these stratigraphic sites. At this time, between  $\sim 6$ –5 ka, the lower portion of Stratigraphic Zone #1 containing sands C and B was deposited (Figure 8, Time 3). The site could have recorded other tsunami sands that eroded or are buried under the present sand ridge, or only two events large enough to overtop the sand barrier occurred before conditions changed. As RSL continued to fall, the coastal barrier, such as the present dunes, would have become an increasingly higher

threshold that tsunamis could not overtop, since RSL fall would have not only increased the relative height of the dunes, but the newly exposed shoreline would have provided a sediment source for dunes to develop. In addition, RSL fall can lead to poorly preserved earthquake and tsunami records, because sea-level fall exposes tsunami deposits preserved within wetland stratigraphy to erosion and bioturbation, leading to thin deposits with low preservation potential (Atwater et al., 1992; Dura et al., 2015, 2016; Nelson et al., 2009).

The question remains, however, why the 1960 tsunami left such widespread, thick deposits across the site when others in the last 5000 years of sea-level fall did not (Figure 8, Time 4). An increase in accommodation space from co-seismic subsidence, or a rise in RSL since 1960, cannot fully explain the selective preservation of the 1960 deposits, as many of the sites remain well above the high-tide elevation. Possibly a relatively recent change in the height or position of the beach ridge and dunes allowed the 1960 tsunami to overtop the previously unexceeded sand barrier. Comparison of aerial

photographs from 1944, 1961, and subsequent years indicates little change in the position of the shoreline in our study area from the bedrock headland at Nigue Sur southward to the tip of the sand spit. However, in the last 70 years the shoreline north of the Nigue Sur bedrock headland (north of the map area in Figure 1) has migrated landward by over 500 m (Figure SI-7), indicating that changes in the coastal geometry are possible on decadal timescales. There is no direct historical or geomorphological evidence to support the idea of human alteration of the sand barrier. The only documented human modification to the dunes occurred after the 1960 tsunami, when they were stabilized with vegetation through government programmes.

A change in the path of the Queule River could also alter sediment supply to the beach and thus affect foredune height evolution (as in Davidson-Arnott et al., 2018). North of the bedrock headland that delineates the northern boundary of our study area at Nigue Sur (Figure 1), paleochannels between the Queule River and the ocean indicate that the river might have taken a different, more direct path to the sea in the past. These paleochannels are almost certainly younger than the RSL high stand, as they appear as low areas in the modern topography and exhibit stratigraphy similar to Nigue Sur in the Queule study area. If the Queule River did discharge elsewhere, the decrease in sediment supply and change in the geometry of the tidal river outlet might either decrease the nearby sand source necessary to create tsunami deposits, or prevent coastal inundation from tsunamis.

The tsunami simulations and eyewitness testimonies from residents all indicate that the 1960 tsunami easily overtopped the elevation of the sand barrier along the entire length of the sand spit and dunes (Figure 3). Subsidence during the 1960 earthquake was estimated as 1.5–1.8 m at Queule (Plafker & Savage, 1970; Wright & Mella, 1963, p. 1374), which would have lowered the minimum elevation required for the tsunami to overtop the coastal sand barrier. We do not know the specific amount of subsidence that occurred at Queule during previous earthquakes, but there is ample historical and geological evidence of subsidence during previous earthquakes at other sites in south-central Chile (Atwater et al., 2013; Cisternas et al., 2005; Cisternas, Carvajal, et al., 2017; Cisternas, Garrett, et al., 2017; Dura et al., 2017; Garrett et al., 2015; Nelson et al., 2009), and therefore a similar pattern would be expected at Queule. However, the simulations of the 1960 tsunami exceeded the elevation of the sand barrier by 2 m, so it would likely have overtopped the barrier even if there had been no subsidence. Thus, we are left with the interpretation that although other factors might have contributed to the absence of tsunami deposits in the >4500 years preceding the 1960 tsunami, it was indeed a particularly large event.

## CONCLUSION

We combined historical documentation, field stratigraphy, and numerical simulations to reconstruct the tsunami record at Queule, Chile, where the giant 1960 earthquake and tsunami destroyed the town. Our 1960 numerical simulations, historical reports, and local eyewitness accounts confirm that the 1960 tsunami overtopped and eroded the coastal sand dunes and inundated all low-lying areas of the Queule vicinity. The 1960 tsunami deposit (sand A) showed an overall landward decrease in median grain size and deposit thickness, with some locations showing local variability in deposit thickness due to

hummocky microtopography. In addition to widespread 1960 tsunami sand deposits, we found two additional older tsunami sand deposits interbedded in organic-rich soils, with maximum ages of 4960–4520 cal BP and 5930–5740. The older tsunami sand deposits (sands B and C) are similar to each other and to the 1960 tsunami sand in their grain size, sharp basal contacts, and tabular geometry, although they are thinner with a shorter landward extent. Sands B and C are among the oldest paleotsunami deposits discovered in southern Chile and contribute to the growing catalogue for this region. Our combined use of historical documentation, 1960 tsunami numerical simulations, and stratigraphy instills confidence in our interpretation of this tsunami record.

Why did the 1960 tsunami leave a ubiquitous depositional record at Queule, whereas no other tsunamis did during the previous >4500 years? The answer is partially attributed to the fall in RSL from the mid- to late Holocene, hindering the creation and preservation of a continuous record of tsunami deposits. Changes in coastal geometry during the latter portion of that time period could have played a role in creating conditions that allowed the 1960 tsunami to overtop the coastal sand barrier. The timing of the establishment of the modern geomorphic setting is unknown, thus we cannot directly compare the magnitude of the 1960 tsunami to others in the past based on the evidence from this single site. However, the 1960 tsunami could have been particularly large at the latitude of Queule based on models of slip distribution.

The influence of the coastal geomorphology and RSL fall on the completeness of the paleotsunami record at Queule is broadly relevant to other similar coastal areas, if paleotsunami records are to be relied on for tsunami hazard assessment. These factors could lead to significant gaps in the tsunami chronology at a single site, which might only be overcome by analysis of multiple locations within a tectonic region. In Chile, numerous historical and geological records indicate that the 1960 earthquake and tsunami were of as great a magnitude and height as any others in coastal records from the region. The depositional record from Queule strengthens the evidence that the 1960 tsunami could be an extremely large, rare event.

## ACKNOWLEDGEMENTS

We would like to thank Diego Aedo, Megan Christie, Tirso Cisternas, Ed Garrett, Fernanda Narbona, and Audrey Piacsek for assistance with field work; Trent Adams, Andrew Deliduka, and Andrew Glenn for contributions to sample processing and grain-size measurements in the lab; and William Manley (INSTAAR, University of Colorado) for providing unpublished stratigraphic data from some of the field sites. We also thank Doña Pachy and Don Jorge from Cabañas Peumayén-Toltén for their hospitality during fieldwork. The manuscript was improved by reviews from S. La Selle, P. Kempf, and an anonymous reviewer. This research project is supported by National Science Foundation (NSF) Awards EAR-1624542 and EAR-1624533, the Millennium Scientific Initiative (ICM) of the Chilean government through Grant NC160025 'Millennium Nucleus CYCLO The Seismic Cycle Along Subduction Zones', Chilean National Fund for Development of Science and Technology (FONDECYT) Grants 1181479 and 1190258, the ANID PIA Anillo ACT192169. Nelson was supported by the Earthquake Hazards Program of the U.S. Geological Survey. Matos-Llavona was also supported by a Puget Sound Energy Graduate Fellowship at Central Washington University. Any use of trade, firm, or product

names is for descriptive purposes only and does not imply endorsement by the U.S. Government.

## AUTHOR CONTRIBUTIONS

PIM-L, LE, and BM took the lead in preparing the manuscript and conceptualized the research. LE, BM, TD, and BPH acquired the main source of funding for this project. PIM-L and BM ran the tsunami numerical simulations. AD, BM, and WS provided the source of one of the tsunami numerical simulations. MC and DM collected fieldwork data and assisted in logistics. RW, MC, TD, and JD surveyed sites and collected field data. WS provided supervision and manuscript revisions. AN, RW, AD, DB, JD, TD, MC, BM, LE, and DM collected field data. JB provided the 1989 interviews. All authors contributed to reviewing and editing the final manuscript.

## DATA AVAILABILITY STATEMENT

The data presented in this paper is made available within the paper itself and the online Supporting Information in graphical and list format. For more information, please contact the corresponding author.

## ORCID

Pedro I. Matos-Llavona  <https://orcid.org/0000-0003-2969-1864>

## REFERENCES

- Abe, K. (1979) Size of great earthquakes of 1837–1974 inferred from tsunami data. *Journal of Geophysical Research*, 84(B4), 1561. Available from: <https://doi.org/10.1029/JB084iB04p01561>
- Aedo, D., Melnick, D., Garrett, E. & Pino, M. (2021) Origen y distribución de depósitos de tsunamis en la marisma de Chaihuín (40° S/73.5° O), Chile. *Andean Geology*, 48(1), 125–152. Available from: <https://doi.org/10.5027/andgeov48n1-3258>
- Alvarez, L. (1963) Studies made between Arauco and Valdivia with respect to the earthquakes of 21 and 22 May 1960. *Bulletin of the Seismological Society of America*, 53(6), 1315–1330. Available from: <https://doi.org/10.1785/BSSA0530061315>
- Angermann, D., Klotz, J. & Reigber, C. (1999) Space-geodetic estimation of the Nazca-South America Euler vector. *Earth and Planetary Science Letters*, 171(3), 329–334. Available from: [https://doi.org/10.1016/S0012-821X\(99\)00173-9](https://doi.org/10.1016/S0012-821X(99)00173-9)
- Arcos, M.E.M. & LeVeque, R.J. (2015) Validating velocities in the GeoClaw tsunami model using observations near Hawaii from the 2011 Tohoku tsunami. *Pure and Applied Geophysics*, 172(3–4), 849–867. Available from: <https://doi.org/10.1007/s00024-014-0980-y>
- Atwater, B.F., Cisternas, M., Yulianto, E., Prendergast, A.L., Jankaew, K., Eipert, A.A., Starin Fernando, W.I., Tejakusuma, I., Schiappacasse, I. & Sawai, Y. (2013) The 1960 tsunamis on beach-ridge plains near Maullín, Chile: Landward descent, renewed breaches, aggraded fans, multiple predecessors. *Andean Geology*, 40(3), 393–418. Available from: <https://doi.org/10.5027/andgeoV40n3-a01>
- Atwater, B.F., Hemphill-Haley, E. 1997. *Recurrence intervals for great earthquakes of the past 3,500 years at northeastern Willapa Bay, Washington*. U.S. Geological Survey Professional Paper 1576. <https://doi.org/10.3133/pp1576>
- Atwater, B.F., Jiménez Nuñez, H. & Vita-Vinzi, C. (1992) Net Holocene emergence despite earthquake-induced submergence, South-Central Chile. *Quaternary International*, 15/16, 77–85. Available from: [https://doi.org/10.1016/1040-6182\(92\)90037-3](https://doi.org/10.1016/1040-6182(92)90037-3)
- Atwater, B.F., Nelson, A.R., Clague, J.J., Carver, G.A., Yamaguchi, D.K., Bobrowsky, P.T., Bourgeois, J., Darienzo, M.E., Grant, W.C., Hemphill-Haley, E., Kelsey, H.M., Jacoby, G.C., Nishenko, S.P., Palmer, S.P., Peterson, C.D. & Reinhart, M.A. (1995) Summary of coastal geologic evidence for past great earthquakes at the Cascadia Subduction Zone. *Earthquake Spectra*, 11(1), 1–18. Available from: <https://doi.org/10.1193/1.1585800>
- Atwater, B.F., Yamaguchi, D.K., Bondevik, S., Barnhardt, W.A., Amidon, L. J., Benson, B.E., Skjerdal, G., Shulene, J.A. & Nanayama, F. (2001) Rapid resetting of an estuarine recorder of the 1964 Alaska earthquake. *Bulletin of the Geological Society of America*, 113(9), 1193–1204. Available from: [https://doi.org/10.1130/0016-7606\(2001\)113<1193:RROAER>2.0.CO;2](https://doi.org/10.1130/0016-7606(2001)113<1193:RROAER>2.0.CO;2)
- Bale, D.S., LeVeque, R.J., Mitran, S. & Rossmanith, J.A. (2003) A wave propagation method for conservation laws and balance laws with spatially varying flux functions. *SIAM Journal on Scientific Computing*, 24(3), 955–978. Available from: <https://doi.org/10.1137/S106482750139738X>
- Barrientos, S.E. & Ward, S.N. (1990) The 1960 Chile earthquake: Inversion for slip distribution from surface deformation. *Geophysical Journal International*, 103(3), 589–598. Available from: <https://doi.org/10.1111/j.1365-246X.1990.tb05673.x>
- Bilek, S.L. (2010) Invited review paper: Seismicity along the South American subduction zone: Review of large earthquakes, tsunamis, and subduction zone complexity. *Tectonophysics*, 495(1–2), 2–14. Available from: <https://doi.org/10.1016/j.tecto.2009.02.037>
- Bourgeois, J. (2009) Geologic effects and records of tsunamis. In: Robinson, A.R. & Bernard, E.N. (Eds.) *The Sea*, Vol. 15. Boston, MA: Harvard University Press, pp. 53–91.
- Bronk Ramsey, C. (2009) Bayesian analysis of radiocarbon dates. *Radiocarbon*, 51(1), 337–360. Available from: <https://doi.org/10.1017/S0033822200033865>
- Cifuentes, I. (1989) The great 1960 Chile earthquakes. *Journal of Geophysical Research*, 94(B1), 665–680. Available from: <https://doi.org/10.1029/JB094iB01p00665>
- Cisternas, M., Atwater, B.F., Torrejón, F., Sawai, Y., Machuca, G., Lagos, M., Eipert, A., Youlton, C., Salgado, I., Kamataki, T., Shishikura, M., Rajendran, C.P., Malik, J.K., Rizal, Y. & Husni, M. (2005) Predecessors of the giant 1960 Chile earthquake. *Nature*, 437(7057), 404–407. Available from: <https://doi.org/10.1038/nature03943>
- Cisternas, M., Carvajal, M., Wesson, R., Ely, L.L. & Gorigoitia, N. (2017) Exploring the historical earthquakes preceding the giant 1960 Chile earthquake in a time-dependent seismogenic zone. *Bulletin of the Seismological Society of America*, 107(6), 2664–2675. Available from: <https://doi.org/10.1785/0120170103>
- Cisternas, M., Garrett, E., Wesson, R., Dura, T. & Ely, L.L. (2017) Unusual geologic evidence of coeval seismic shaking and tsunamis shows variability in earthquake size and recurrence in the area of the giant 1960 Chile earthquake. *Marine Geology*, 385, 101–113. Available from: <https://doi.org/10.1016/j.margeo.2016.12.007>
- Clark, K., Howarth, J., Litchfield, N., Cochran, U., Turnbull, J., Dowling, L., Howell, A., Berryman, K. & Wolfe, F. (2019) Geological evidence for past large earthquakes and tsunamis along the Hikurangi subduction margin, New Zealand. *Marine Geology*, 412, 139–172. Available from: <https://doi.org/10.1016/j.margeo.2019.03.004>
- Clawpack Development Team. 2017. Clawpack vers. 5.4.0. <https://doi.org/10.5281/ZENODO.262111>
- Davidson-Arnott, R., Hesp, P., Ollerhead, J., Walker, I., Bauer, B., Delgado-Fernandez, I. & Smyth, T. (2018) Sediment budget controls on fore-dune height: Comparing simulation model results with field data. *Earth Surface Processes and Landforms*, 43(9), 1798–1810. Available from: <https://doi.org/10.1002/esp.4354>
- Dillehay, T.D., Quivira, M.P., Bonzani, R., Silva, C., Wallner, J. & Le Quesne, C. (2007) Cultivated wetlands and emerging complexity in south-central Chile and long distance effects of climate change. *Antiquity*, 81(314), 949–960. Available from: <https://doi.org/10.1017/S0003598X00096034>
- Dolcimascolo A. 2019. *Defining historical earthquake rupture parameters and proposed slip distributions through tsunami modeling in south-central Chile*. Master's thesis, Central Washington University. <https://digitalcommons.cwu.edu/etd/1200>
- Duke, C.M. & Leeds, D.J. (1963) Response of soils, foundations, and earth structures to the Chilean earthquakes of 1960. *Bulletin of the Seismological Society of America*, 53(2), 309–357. Available from: <https://doi.org/10.1785/BSSA0530020309>
- Dura, T., Cisternas, M., Horton, B.P., Ely, L.L., Nelson, A.R., Wesson, R.L. & Pilarczyk, J.E. (2015) Coastal evidence for Holocene subduction-zone

- earthquakes and tsunamis in central Chile. *Quaternary Science Reviews*, 113, 93–111. Available from: <https://doi.org/10.1016/j.quascirev.2014.10.015>
- Dura, T., Engelhart, S.E., Vacchi, M., Horton, B.P., Kopp, R.E., Peltier, W. R. & Bradley, S. (2016) The role of Holocene relative sea-level change in preserving records of subduction zone earthquakes. *Current Climate Change Reports*, 2(3), 86–100. Available from: <https://doi.org/10.1007/s40641-016-0041-y>
- Dura, T., Horton, B.P., Cisternas, M., Ely, L.L., Hong, I., Nelson, A.R., Wesson, R.L., Pilarczyk, J.E., Parnell, A.C. & Nikitina, D. (2017) Subduction zone slip variability during the last millennium, south-central Chile. *Quaternary Science Reviews*, 175, 112–137. Available from: <https://doi.org/10.1016/j.quascirev.2017.08.023>
- Eaton, J.P., Richter, D.H. & Ault, W.U. (1961) The tsunami of May 23, 1960, on the Island of Hawaii. *Bulletin of the Seismological Society of America*, 51(2), 135–157. Available from: <https://doi.org/10.1785/BSSA0510020135>
- Egbert, G.D. & Erofeeva, S.Y. (2002) Efficient inverse modeling of barotropic ocean tides. *Journal of Atmospheric and Oceanic Technology*, 19(2), 183–204. Available from: [https://doi.org/10.1175/1520-0426\(2002\)019%3C0183:EIMOBO%3E2.0.CO;2](https://doi.org/10.1175/1520-0426(2002)019%3C0183:EIMOBO%3E2.0.CO;2)
- Ely, L.L., Cisternas, M., Wesson, R.L. & Dura, T. (2014) Five centuries of tsunamis and land-level changes in the overlapping rupture area of the 1960 and 2010 Chilean earthquakes. *Geology*, 42(11), 995–998. Available from: <https://doi.org/10.1130/G35830.1>
- Fritz, H.M., Petroff, C.M., Catalán, P.A., Cienfuegos, R., Winckler, P., Kalligeris, N., Weiss, R., Barrientos, S.E., Meneses, G., Valderas-Bermejo, C., Ebeling, C., Papadopoulos, A., Contreras, M., Almar, R., Dominguez, J.C. & Synolakis, C.E. (2011) Field survey of the 27 February 2010 Chile tsunami. *Pure and Applied Geophysics*, 168(11), 1989–2010. Available from: <https://doi.org/10.1007/s00024-011-0283-5>
- Fujii, Y. & Satake, K. (2013) Slip distribution and seismic moment of the 2010 and 1960 Chilean earthquakes inferred from tsunami waveforms and coastal geodetic data. *Pure and Applied Geophysics*, 170(9–10), 1493–1509. Available from: <https://doi.org/10.1007/s00024-012-0524-2>
- Garrett, E., Melnick, D., Dura, T., Cisternas, M., Ely, L.L., Wesson, R.L., Jaramuñoz, J. & Whitehouse, P.L. (2020) Holocene relative sea-level change along the tectonically active Chilean coast. *Quaternary Science Reviews*, 236, 106281. Available from: <https://doi.org/10.1016/j.quascirev.2020.106281>
- Garrett, E., Shennan, I., Woodroffe, S.A., Cisternas, M., Hocking, E.P. & Gulliver, P. (2015) Reconstructing paleoseismic deformation, 2: 1000 years of great earthquakes at Chucalén, south central Chile. *Quaternary Science Reviews*, 113, 112–122. Available from: <https://doi.org/10.1016/j.quascirev.2014.10.010>
- González FI, LeVeque RJ, Chamberlain P, Hirai B, Varkovitzky J, George DL. 2011. Validation of the GeoClaw model. In *Proceedings of the NTHMP MMS Tsunami Inundation Model Validation Workshop*, Galveston, TX. <https://depts.washington.edu/clawpack/links/nthmp-benchmarks/geoclaw-results.pdf>
- Hocking, E.P., Garrett, E., Aedo, D., Carvajal, M. & Melnick, D. (2021) Geological evidence of an unreported historical Chilean tsunami reveals more frequent inundation. *Communications Earth & Environment*, 2(1), 1–10. Available from: <https://doi.org/10.1038/s43247-021-00319-z>
- Hogg, A.G., Heaton, T.J., Hua, Q., Palmer, J.G., Turney, C.S.M., Southon, J., Bayliss, A., Blackwell, P.G., Boswijk, G., Bronk Ramsey, C., Pearson, C., Petchey, F., Reimer, P., Reimer, R. & Wacker, L. (2020) SHCal20 Southern Hemisphere Calibration, 0–55,000 years cal BP. *Radiocarbon*, 62(4), 759–778. Available from: <https://doi.org/10.1017/RDC.2020.59>
- Hong, I., Dura, T., Ely, L.L., Horton, B.P., Nelson, A.R., Cisternas, M., Nikitina, D. & Wesson, R.L. (2017) A 600-year-long stratigraphic record of tsunamis in south-central Chile. *Holocene*, 27(1), 39–51. Available from: <https://doi.org/10.1177/0959683616646191>
- Kemp, A.C., Nelson, A.R. & Horton, B.P. (2013) Radiocarbon dating of plant macrofossils from tidal-marsh sediment. In: Shroder, J.F. (Ed.) *Treatise on Geomorphology*, Vol. 14. New York: Academic Press, pp. 370–388. Available from: <https://doi.org/10.1016/B978-0-12-374739-6.00400-0>
- Kempf, P., Moernaut, J., van Daele, M., Pino, M., Urrutia, R. & de Batist, M. (2020) Paleotsunami record of the past 4300 years in the complex coastal lake system of Lake Cucao, Chiloé Island, south central Chile. *Sedimentary Geology*, 401, 105644. Available from: <https://doi.org/10.1016/j.sedgeo.2020.105644>
- Kempf, P., Moernaut, J., van Daele, M., Vandoorne, W., Pino, M., Urrutia, R. & de Batist, M. (2017) Coastal lake sediments reveal 5500 years of tsunami history in south central Chile. *Quaternary Science Reviews*, 161, 99–116. Available from: <https://doi.org/10.1016/j.quascirev.2017.02.018>
- Kempf, P., Moernaut, J., van Daele, M., Vermassen, F., Vandoorne, W., Pino, M., Urrutia, R., Schmidt, S., Garrett, E. & de Batist, M. (2015) The sedimentary record of the 1960 tsunami in two coastal lakes on Isla de Chiloé, south central Chile. *Sedimentary Geology*, 328, 73–86. Available from: <https://doi.org/10.1016/j.sedgeo.2015.08.004>
- Leveque, R.J., George, D.L. & Berger, M.J. (2011) Tsunami modelling with adaptively refined finite volume methods. *Acta Numerica*, 20, 211–289. Available from: <https://doi.org/10.1017/S0962492911000043>
- Lomnitz, C. (2004) Major earthquakes of Chile: A historical survey, 1535–1960. *Seismological Research Letters*, 75(3), 368–378. Available from: <https://doi.org/10.1785/gssrl.75.3.368>
- MacInnes, B.T., Weiss, R., Bourgeois, J. & Pinegina, T.K. (2010) Slip distribution of the 1952 Kamchatka great earthquake based on near-field tsunami deposits and historical records. *Bulletin of the Seismological Society of America*, 100(4), 1695–1709. Available from: <https://doi.org/10.1785/0120090376>
- Melnick, D., Bookhagen, B., Strecker, M.R. & Echtler, H.P. (2009) Segmentation of megathrust rupture zones from fore-arc deformation patterns over hundreds to millions of years, Arauco peninsula, Chile. *Journal of Geophysical Research - Solid Earth*, 114(B1), B01407. Available from: <https://doi.org/10.1029/2008JB005788>
- Minoura, K. & Nakaya, S. (1991) Traces of tsunami preserved in inter-tidal lacustrine and marsh deposits: Some examples from northeast Japan. *Journal of Geology*, 99(2), 265–287. Available from: <https://doi.org/10.1086/629488>
- Moernaut, J., van Daele, M., Fontijn, K., Heirman, K., Kempf, P., Pino, M., Valdebenito, G., Urrutia, R., Strasser, M. & de Batist, M. (2018) Larger earthquakes recur more periodically: New insights in the megathrust earthquake cycle from lacustrine turbidite records in south-central Chile. *Earth and Planetary Science Letters*, 481, 9–19. Available from: <https://doi.org/10.1016/j.epsl.2017.10.016>
- Moernaut, J., van Daele, M., Heirman, K., Fontijn, K., Strasser, M., Pino, M., Urrutia, R. & de Batist, M. (2014) Lacustrine turbidites as a tool for quantitative earthquake reconstruction: New evidence for a variable rupture mode in south central Chile. *Journal of Geophysical Research - Solid Earth*, 119(3), 1607–1633. Available from: <https://doi.org/10.1002/2013JB010738>
- Moore, A.L., McAdoo, B.G. & Ruffman, A. (2007) Landward fining from multiple sources in a sand sheet deposited by the 1929 Grand Banks tsunami, Newfoundland. *Sedimentary Geology*, 200(3–4), 336–346. Available from: <https://doi.org/10.1016/j.sedgeo.2007.01.012>
- Moreno, M., Melnick, D., Rosenau, M., Bolte, J., Klotz, J., Echtler, H., Baez, J., Bataille, K., Chen, J., Bevis, M., Hase, H. & Oncken, O. (2011) Heterogeneous plate locking in the South-Central Chile subduction zone: Building up the next great earthquake. *Earth and Planetary Science Letters*, 305(3–4), 413–424. Available from: <https://doi.org/10.1016/j.epsl.2011.03.025>
- Moreno, M.S., Bolte, J., Klotz, J. & Melnick, D. (2009) Impact of megathrust geometry on inversion of coseismic slip from geodetic data: Application to the 1960 Chile earthquake. *Geophysical Research Letters*, 36(16), L16310. Available from: <https://doi.org/10.1029/2009GL039276>
- Morton, R.A., Gelfenbaum, G. & Jaffe, B.E. (2007) Physical criteria for distinguishing sandy tsunamis and storm deposits using modern examples. *Sedimentary Geology*, 200(3–4), 184–207. Available from: <https://doi.org/10.1016/j.sedgeo.2007.01.003>
- National Centers for Environmental Information. 2019. *Global Historical Tsunami Database*. National Oceanic and Atmospheric



- Administration/World Data Service. <https://doi.org/10.7289/V5PN93H7>
- Nelson, A.R. (2015) Chapter 4: Coastal sediments. In: Shennan, I., Ling, A. J. & Horton, B.P. (Eds.) *Handbook of Sea-Level Research*. Chichester: Wiley, pp. 47–65. Available from: <https://doi.org/10.1002/9781118452547.ch4>
- Nelson, A.R., DuRoss, C.B., Witter, R.C., Kelsey, H.M., Engelhart, S.E., Mahan, S.A., Gray, H.J., Hawkes, A.D., Horton, B.P. & Padgett, J.S. (2021) A maximum rupture model for the central and southern Cascadia subduction zone—reassessing ages for coastal evidence of megathrust earthquakes and tsunamis. *Quaternary Science Reviews*, 261, 106922. Available from: <https://doi.org/10.1016/j.quascirev.2021.106922>
- Nelson, A.R., Kashima, K. & Bradley, L.A. (2009) Fragmentary evidence of great-earthquake subsidence during Holocene emergence, Valdivia estuary, south central Chile. *Bulletin of the Seismological Society of America*, 99(1), 71–86. Available from: <https://doi.org/10.1785/0120080103>
- Nelson, A.R., Shennan, I. & Long, A.J. (1996) Identifying coseismic subsidence in tidal-wetland stratigraphic sequences. *Journal of Geophysical Research*, 101(B3), 6115–6135. Available from: <https://doi.org/10.1029/95JB01051>
- OEA-Chile. 1961–1962. Proyecto Aerofotogramétrico OEA-Chile, 1: 50.000, January 1961–February 1962.
- Peters, R. & Jaffe, B. 2010. *Identification of tsunami deposits in the geologic record; developing criteria using recent tsunami deposits*. U.S. Geological Survey Open-File Report 2010–1239. <https://doi.org/10.3133/ofr20101239>
- Philibosian, B. & Meltzner, A.J. (2020) Segmentation and supercycles: A catalog of earthquake rupture patterns from the Sumatran Sunda Megathrust and other well-studied faults worldwide. *Quaternary Science Reviews*, 241, 106390. Available from: <https://doi.org/10.1016/j.quascirev.2020.106390>
- Pino, M.Q. & Muslow, S.F. (1983) Distribucion de facies granulométricas en el estuario del río Queule, IX Region: Un análisis de componentes principales. *Revista Geologica de Chile*, 18(1), 77–85 (in Spanish). Available from: <https://doi.org/10.5027/andgeoV10n1-a05>
- Plafker, G. & Savage, J.C. (1970) Mechanism of the Chilean earthquakes of May 21 and 22, 1960. *Bulletin of the Geological Society of America*, 81(4), 1001–1030. Available from: [https://doi.org/10.1130/0016-7606\(1970\)81\[1001:MOTCEO\]2.0.CO;2](https://doi.org/10.1130/0016-7606(1970)81[1001:MOTCEO]2.0.CO;2)
- Reinhardt, E.G., Nairn, R.B. & Lopez, G. (2009) Recovery estimates for the Río Cruces after the May 1960 Chilean earthquake. *Marine Geology*, 269(1–2), 18–33. Available from: <https://doi.org/10.1016/j.margeo.2009.12.003>
- Rohas, C.H. (1986) El estuario del río Queule: Un ambiente sedimentario en el Sur de Chile. *Anales Del Centro de Ciencias Del Mar Y Limnología*, 13, 231–240. (in Spanish).
- Rubin, C.M., Horton, B.P., Sieh, K., Pilarczyk, J.E., Daly, P., Ismail, N. & Parnell, A.C. (2017) Highly variable recurrence of tsunamis in the 7,400 years before the 2004 Indian Ocean tsunami. *Nature Communications*, 8(1), 16019. Available from: <https://doi.org/10.1038/ncomms16019>
- Ruiz, S. & Madariaga, R. (2018) Historical and recent large megathrust earthquakes in Chile. *Tectonophysics*, 733, 37–56. Available from: <https://doi.org/10.1016/j.tecto.2018.01.015>
- Satake, K. & Atwater, B.F. (2007) Long-term perspectives on giant earthquakes and tsunamis at subduction zones. *Annual Review of Earth and Planetary Sciences*, 35(1), 349–374. Available from: <https://doi.org/10.1146/annurev.earth.35.031306.140302>
- Sawai, Y. (2020) Subduction zone paleoseismology along the Pacific coast of northeast Japan – progress and remaining problems. *Earth-Science Reviews*, 208, 103261. Available from: <https://doi.org/10.1016/j.earscirev.2020.103261>
- Sawai, Y., Namegaya, Y., Okamura, Y., Satake, K. & Shishikura, M. (2012) Challenges of anticipating the 2011 Tohoku earthquake and tsunami using coastal geology. *Geophysical Research Letters*, 39(21), L21309. Available from: <https://doi.org/10.1029/2012GL053692>
- Shennan, I., Barlow, N., Combellick, R., Pierre, K. & Stuart-Taylor, O. (2014) Late Holocene paleoseismology of a site in the region of maximum subsidence during the 1964 Mw 9.2 Alaska earthquake. *Journal of Quaternary Science*, 29(4), 343–350. Available from: <https://doi.org/10.1002/jqs.2705>
- Shennan, I., Garrett, E. & Barlow, N. (2016) Detection limits of tidal-wetland sequences to identify variable rupture modes of megathrust earthquakes. *Quaternary Science Reviews*, 150, 1–30. Available from: <https://doi.org/10.1016/j.quascirev.2016.08.003>
- Sievers, C.H.A., Villegas, C.G., Barros, G. & Saint-Amand, P. (1963) The seismic sea wave of 22 May 1960 along the Chilean coast. *Bulletin of the Seismological Society of America*, 53(6), 1125–1190. Available from: <https://doi.org/10.1785/BSSA0530061125>
- Synolakis, C.E., Bernard, E.N., Titov, V., Kânoğlu, U. & González, F.I. (2008) Validation and verification of tsunami numerical models. *Pure and Applied Geophysics*, 165(11–12), 2197–2228. Available from: <https://doi.org/10.1007/s00024-004-0427-y>
- Szczuciński, W. (2012) The post-depositional changes of the onshore 2004 tsunami deposits on the Andaman Sea coast of Thailand. *Natural Hazards*, 60(1), 115–133. Available from: <https://doi.org/10.1007/s11069-011-9956-8>
- Troels-Smith, J. (1955) *Characterization of unconsolidated sediments*, Geological Survey of Denmark, Series IV, Vol. 3, No. 10. Copenhagen: Reitzel.
- Watanabe, T. & Kokot, J. (1960) Los movimientos sísmicos del mes de mayo de 1960 en Chile. *Anales de La Facultad de Ciencias Y Matemáticas*, 17(17), 39–87. (in Spanish).
- Weischet, W. (1960) Contribuciones al estudio de las transformaciones geográficas en la parte septentrional del sur de Chile por efecto del sismo del 22 de Mayo del 1960. *Anales de la Facultad de Ciencias Físicas y Matemáticas*, 17(17), 91–132. (in Spanish).
- Weischet, W. (1963) Further observations of geologic and geomorphic changes resulting from the catastrophic earthquake of May 1960, in Chile. *Bulletin of the Seismological Society of America*, 53(6), 1237–1257. Available from: <https://doi.org/10.1785/BSSA0530061237>
- Witter, R., Briggs, R., Engelhart, S.E., Gelfenbaum, G., Koehler, R.D., Nelson, A., la Selle, S.P., Corbett, R. & Wallace, K. (2019) Evidence for frequent, large tsunamis spanning locked and creeping parts of the Aleutian megathrust. *Bulletin of the Geological Society of America*, 131(5–6), 707–729. Available from: <https://doi.org/10.1130/B32031.1>
- Wright, C. & Mella, A. (1963) Modifications to the soil pattern of south-central Chile resulting from seismic and associated phenomena during the period May to August 1960. *Bulletin of the Seismological Society of America*, 53(6), 1367–1402. Available from: <https://doi.org/10.1785/BSSA0530061367>
- Zayakin, Y.A. & Luchinina, A.A. (1987) *Catalogue of tsunamis on Kamchatka*. Obninsk: Vniigni-Mtsd (in Russian).

## SUPPORTING INFORMATION

Additional supporting information may be found in the online version of the article at the publisher's website.

**How to cite this article:** Matos-Llavona, P.I., Ely, L.L., MacInnes, B., Dura, T., Cisternas, M.A., Bourgeois, J. et al. (2022) The giant 1960 tsunami in the context of a 6000-year record of paleotsunamis and coastal evolution in south-central Chile. *Earth Surface Processes and Landforms*, 1–17. Available from: <https://doi.org/10.1002/esp.5363>